NSF/RANN AER 74-02094 SR-2/75
ESD-TR-76-29

FG

12

See 1473

Semiannual Technical Summary

Solid Electrolytes: Alkali-Ion Transport in Skeleton Structures

31 December 1975

Prepared for the National Science Foundation
under NSF/RANN Contract AER 74-02094
and for the Defense Advanced Research Projects Agency
under Electronic Systems Division Contract F19628-76-C-0002 by

Lincoln Laboratory
MASSACHUSETTS INSTITUTE OF TECHNOLOGY
LEXINGTON, MASSACHUSETTS

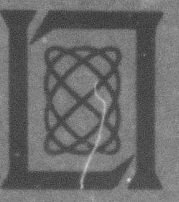

The work reported in this document was performed at Lincoln Laboratory, a center for research operated by Massachusetts Institute of Technology. This work was sponsored by the National Science Foundation under NSF/RANN Contract AER 74-02094 and by the Defense Advanced Research Projects Agency under Air Force Contract F19628-76-C-0002 (ARPA Order 2696).

This report was prepared with the support of NSF Grant No. AER 74-02094. Any opinions, findings, conclusions or recommendations expressed herein are those of the contractor and do not necessarily reflect the views of the National Science Foundation.

This technical report has been reviewed and is approved for publication.

FOR THE COMMANDER

Eugene C. Raabe

Eugene C. Raabe, Lt. Col., USAF
Chief, ESD Lincoln Laboratory Project Office

MASSACHUSETTS INSTITUTE OF TECHNOLOGY

LINCOLN LABORATORY

SOLID ELECTROLYTES: ALKALI-ION TRANSPORT IN SKELETON STRUCTURES

SEMIANNUAL TECHNICAL SUMMARY REPORT
TO THE
NATIONAL SCIENCE FOUNDATION
AND TO THE
DEFENSE ADVANCED RESEARCH PROJECTS AGENCY

1 JULY – 31 DECEMBER 1975

ISSUED 11 FEBRUARY 1976

LEXINGTON MASSACHUSETTS

ABSTRACT

We have demonstrated the existence of fast, three-dimensional Na^+-ion transport in the system $Na_{1+3y}Zr_2(P_{1-y}Si_yO_4)_3$ for $0 \leq y \leq 1$, and we have shown that the structure consists of a rigid skeleton of tetrahedra sharing corners with octahedra, octahedra with tetrahedra, having an interconnected interstitial space with four Na^+-ion positions per formula unit. The Na^+-ion positions are not crystallographically equivalent: M_I positions are octahedrally coordinated by M_{II} positions, which form close-packed sheets in the basal planes of an hexagonal ($R\bar{3}c$) unit cell; M_{II} positions have two near-neighbor M_I positions, one in each of the neighboring basal planes. The $M_I + 3M_{II}$ matrix has only M_I sites occupied in $NaZr_2(PO_4)_3$, all sites occupied in $Na_4Zr_2(SiO_4)_3$. A distortion from hexagonal to orthorhombic C2/c symmetry occurs in a narrow compositional range about $Na_3Zr_2PSi_2O_{12}$, but the distortion has little apparent influence on the Na^+-ion mobility. At 300°C, the operating temperature of a Na-S battery, the resistivity (5 Ω-cm) for Na^+-ion transport in $Na_3Zr_2PSi_2O_{12}$ is competitive with the best β''-alumina. The activation energy for Na^+-ion transport, about 0.26 eV, is about 0.08 eV higher than that of β''-alumina, which makes this compound superior to the best β''-alumina at temperatures greater than 300°C, inferior at lower temperatures. The compound is stable in molten sodium and can be sintered at 1250°C. We have elected to concentrate on the fabrication of ceramic cups suitable for cell construction in order to test the chemical stability of this compound under the operating conditions of a Na-S cell.

CONTENTS

SOLID ELECTROLYTES: ALKALI-ION TRANSPORT IN SKELETON STRUCTURES

1. SUMMARY

The essential strategy of our search for fast alkali-ion conduction in skeleton structures is presented in Sec. II; and the structure determination of the most important system discovered to date, $Na_{1+3y}Zr_2(P_{1-y}Si_yO_4)_3$, is presented in Sec. III. These two sections represent papers that will be published in the February 1976 issue of the Materials Research Bulletin.

The compound $Na_3Zr_2PSi_2O_{12}$ (Nazirpsio) has a Na^+-ion conductivity that is competitive with the best β"-alumina at the operating temperatures of a Na-S battery. Whereas β" supports Na^+-ion conductivity in only widely separated layers, $Na_3Zr_2PSi_2O_{12}$ supports three-dimensional Na^+-ion transport. Therefore, whereas β" has the smaller activation energy for Na^+-ion transport ($\epsilon_a \approx 0.18$ eV vs 0.26 eV), it also has the smaller pre-exponential factor in the conductivity expression

$$\sigma \approx (Ne^2/kT)\, c(1-c)\, z a_\ell^2 \nu_o \exp(\Delta S/k) \exp(-\epsilon_a/kT)$$

where N is the density of available Na^+-ion sites, c is the Na^+-ion concentration, z is the average number of nearest neighbor sites separated a distance a_ℓ, ν_o is the jump-attempt frequency at temperatures $T >> \epsilon_a/k$, and $\epsilon_a - T\Delta S$ is the Gibbs free energy that must be supplied thermally to activate a jump.

The excellent properties of Nazirpsio have caused us to split our effort into two parts: (1) a continuation of the search for improved Na^+-ion conduction in skeleton structures, and (2) the development of Nazirpsio as a competitor to β"-alumina. In the first of these efforts, we have turned again to the Carnegieite structure of high-temperature $NaAlSiO_4$, which contains a skeleton of corner-shared tetrahedra. In the second, we are initially concentrating on the preparation of dense ceramic cups and of dense ceramic disks sealed into glass U-tubes for definitive measurements of Na^+-ion transport and of chemical stability as a function of charging and discharging current densities. Appropriate life tests will also be initiated.

Sample preparation: Fabrication of dense ceramic membranes of $Na_3Zr_2PSi_2O_{12}$ promises to be easier and more straightforward than the production of β"-alumina membranes of comparable quality. We have, for example, consistently produced disks of 91 to 94 percent theoretical density by firing cold-pressed disks to 1225°C in air for 3 hours. We have also produced both open and closed-ended tubes of Nazirpsio by the same heat treatment of cold-formed tubes. The quality of the tubes was improved by isostatic pressing before firing. With either procedure, tubes of greater than 90 percent theoretical density are obtained.

An advantage of this material is that it can be held at sintering temperatures for long periods without any apparent loss of sodium.

All the conductivity measurements reported to date have been made on unsealed specimens sintered in air. Three specimens that were hot forged at 1150°C exhibited densities of about 97 percent theoretical.

We plan to proceed with the development of fabrication techniques for achieving ultimate densities not only of disks, but of any arbitrary shape such as a tube, a cup, or a corrogated slab. The optimum initial particle size is presently under investigation.

Sodium-sodium cell: We have made a successful, though brief, DC measurement of Na^+-ion conductivity at high current density in a Na-Na cell. This is a significant result; it demonstrates that the in situ vacuum-fill technique used does indeed prevent the formation of a resistive film at the sodium-electrolyte interface, a problem that has plagued previous workers in the field. The research group at the Ford Motor Co., for example, have used Na-Na cells for testing samples of β-alumina, but not for a reliable determination of intrinsic electrical properties. In contrast, we should be able to combine conductivity measurements with lifetime evaluation in a Na-Na cell.

Our design of a sodium-sodium cell began with an investigation of the lifetimes of epoxy cements at temperatures $T < 300°C$. A disk of nominal composition $Na_3Zr_2PSi_2O_{12}$ was sealed into a Vycor tube with Epoxy Patch (a product of the Hysol Division of the Dexter Corporation) and was mounted into our Na-Na cell, which was then charged with liquid sodium using the procedure described in the previous semiannual report. Particular pains were taken to ensure that both the ceramic and Vycor surfaces were completely wetted by the epoxy and that no bubbles were present in the seal. Voltage-current measurements were made at several temperatures from 140 to 280°C. The absence of any frequency dependence was established by using a Tektronix oscilloscope to observe the current flowing in response to the application of a square-wave voltage across the Na-Na cell. This result demonstrated the absence of any contamination film at the sodium-ceramic interface. However, the response to DC excitation showed a marked polarity dependence that was apparently due to the formation and trapping of a sodium-vapor bubble underneath the sample. In order to avoid this difficulty in the future, we are developing a U-tube cell in which the disk-shaped electrolyte is mounted vertically – rather than horizontally – in the center, thereby ensuring equivalence of the two disk surfaces. Moreover, a ceramic-to-glass seal is being developed to replace the epoxy since subsequent examination of the sealing epoxy showed significant decomposition even at the modest temperatures employed for our experiments.

In order to develop a satisfactory ceramic-to-glass seal, the diametrical thermal expansion of the ceramic disks was measured. The sample was positioned on edge in the middle of a thimble-sized furnace by means of a piece of fused quartz of very low thermal expansion. The furnace rested on an aluminum block that was sufficiently massive to remain at constant temperature during the measurement. A movable mirror, pivoted from an extension of the reference surface, was supported by a second piece of fused quartz resting on the upper edge of the sample disk. Expansion of the sample moved the mirror about its pivot point, and the deflection was amplified by multiple reflections of the beam from a helium-neon alignment laser between the movable mirror and a stationary one. We found it essential to prevent any rolling motion of the samples. Using this arrangement, we were able to duplicate the literature values for the thermal-expansion coefficients of Vycor ($\alpha = 0.8 \times 10^{-6}/°C$), soft glass ($9.2 \times 10^{-6}/°C$), cold-rolled steel ($12 \times 10^{-6}/°C$), and brass ($18.5 \times 10^{-6}/°C$). For Nazirpsio we obtained a best value of $\alpha = 6.7 \pm 0.4 \times 10^{-6}/°C$. This closely approximates the value of $6.4 \times 10^{-6}/°C$ given for the Corning Code 7280 alkali-resistant glass. Preliminary seals have demonstrated that 7280 glass forms an excellent, virtually strain-free bond to Nazirpsio ceramic disks.

A special electronic driver for use with Na-Na cells was designed and constructed. It features four independent output drivers, each of which can drive a Na-Na cell at preset current levels of 1.0, 0.5, 0.25, and 0.125 A with 1-percent accuracy and 5-V compliance. The use of current control provides easy monitoring of cell resistance and automatic protection against

short-circuit eell failure. Relays, driven from an internal eloek, reverse the output polarity after time intervals that ean be preset to values between 15 min. and 24 hours. This provision is required for life testing beeause the passage of 1 A of eurrent for a period of 1 hour transports approximately 1 ee of liquid sodium through the sample. Our present cell was designed for approximately 2 cc of liquid in the inner tube; the new U-tube cell for twice as much on eaeh side.

A Nazirpsio disk was suecessfully sealed in a 7280 tube, but the glass eraeked when a string saw was used to make a eut right at the sample. Through a misunderstanding, a butt seal was made to another Nazirpsio disk. Although such a seal is inherently less secure, we mounted it in the Na-Na eell and attempted a run using the driver described above. A current of 0.5 A was passed through the sample, and resistance values of 2.75, 2.60, and 2.45 Ω were measured at 240, 248, and 253°C, respeetively, indicating an aetivation energy of 0.20 eV. Extrapolation with this value would yield a resistanee of 1.71 Ω at 300°C and, guessing the surfaee area inside the glass seal to be 0.75 cm^2, a resistivity of about 5 Ω-cm. Upon reversing polarity, the resistance appeared to increase by about 0.3 Ω. At 270°C, we measured the voltage drop across the eell at all four preset current levels from 0.125 to 1.0 A. The eurrent-voltage graph shows truly ohmie behavior over this entire range with an overpotential of 30 mV, which may be due to our eontaet eleetrodes. The seal failed before further measurements could be made. It is possible that the 1-A eurrent level eontributed to its failure.

Despite its brevity, the above run was a notable success. We made a DC measurement at a high current density in a Na-Na eell and obtained values for the resistivity that agree with those previously found by high-frequency AC techniques. We expect to make many more measurements in sodium-sodium eells during the next six months. We plan to establish whether Nazirpsio suffers any eleetrical degradation from prolonged exposure to liquid sodium and how any such degradation might depend upon the eurrent density imposed upon it. Our next step will be to construct a Na-S eell to determine the ehemical stability of Nazirpsio under normal operating conditions.

II. PAPER TO APPEAR FEBRUARY ISSUE OF MATERIALS RESEARCH BULLETIN

FAST Na^+-ION TRANSPORT IN SKELETON STRUCTURES*

J. B. Goodenough, H. Y-P. Hong, and J. A. Kafalas
Lincoln Laboratory, Massachusetts Institute of Technology
Lexington, Massachusetts 02173

ABSTRACT

Skeleton structures have been explored experimentally for fast Na^+-ion transport. A skeleton structure consists of a rigid skeletal array of atoms stabilized by electrons donated by alkali ions partially occupying sites in a three dimensionally linked interstitial space. Fast Na^+-ion transport was demonstrated in several structures, and the system $Na_{1+x}Zr_2P_{3-x}Si_xO_{12}$ has a Na^+-ion resistivity at 300°C of $\rho_{300} \lesssim 5\Omega$-cm for $x \approx 2$, which is competitive with the best β''-alumina. An activation energy $\delta_a \approx 0.29$ eV is about 0.1 eV larger than that of β''-alumina.

Introduction

The discovery[1] of fast Na^+-ion transport in β- and β''-alumina has stimulated interest in the use of solid electrolytes in cells and thermoelectric generators.[2] The best compositions have resistivities for fast Na^+-ion transport at 300°C of $\rho_{300} = 4\Omega$-cm with an activation energy for the mobility $\delta_a = 0.16$ eV[3]. The volatility of sodium together with the refractory character of Al_2O_3 has made awkward economic fabrication of ceramic membranes, but this problem appears to be solved.[4] Nevertheless, β- and β''-alumina are layer compounds in which the Na^+ ions are constrained to move in only two dimensions. Anisotropic thermal expansion[5] can reduce the life of thermally cycled membranes, and confinement of the Na^+ ions to widely separated layers reduces sharply the fraction of the membrane volume that transports Na^+ ions. Therefore, the design of a material that can provide equivalently fast Na^+-ion transport in three dimensions has challenged solid state chemists. We report here on a strategy and related experiments that have enabled us to meet this challenge.

Skeleton Structures

Our strategy was to investigate alkali-ion transport in cubic "skeleton" structures. A skeleton structure consists of a rigid subarray with interconnected interstitial space in which ions move in three dimensions. Ionic mobility requires the existence of an interconnected space of partially occupied lattice sites having equivalent (or nearly so) site-occupation energies. For fast ion transport, the activation energy for an ion jump from one site to another must be small. Therefore, the site-interface "bottlenecks," whether shared faces or shared edges, must be open enough for easy ion passage.

*This work was sponsored by the Defense Advanced Research Projects Agency, NASA, and NSF/RANN.

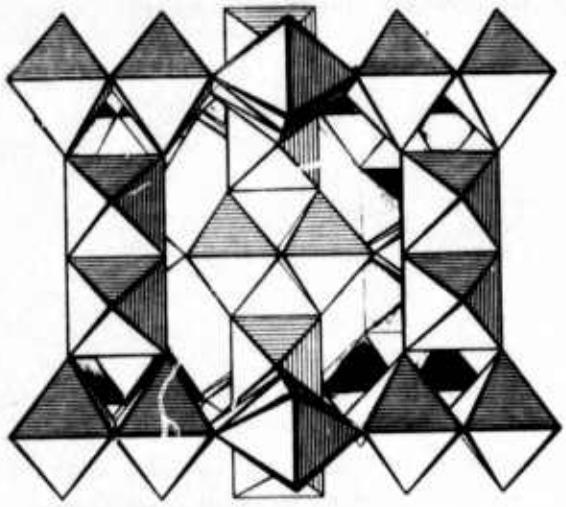

Fig. 1
The $(SbO_3)^-$ array of cubic $KSbO_3$.

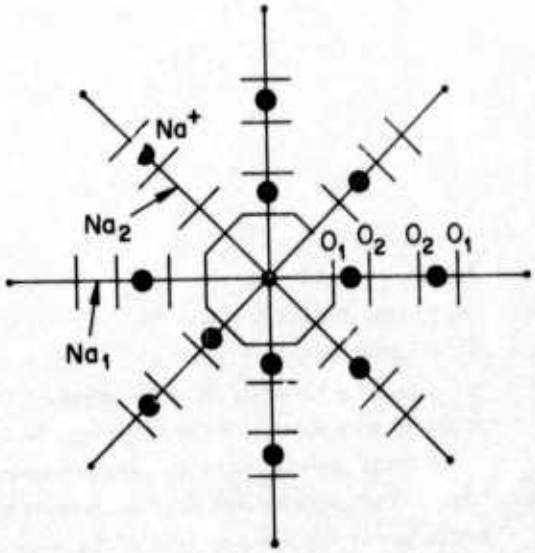

Fig. 2
Schematization of the eight ⟨111⟩ tunnel segments from the origin to neighboring body-centered positions in Im 3-cubic $KSbO_3$. In the ordered Pn3 structure, each singly occupied branch has an M_2 cation and the nearest-neighbor branches are doubly occupied by M_1 cations.

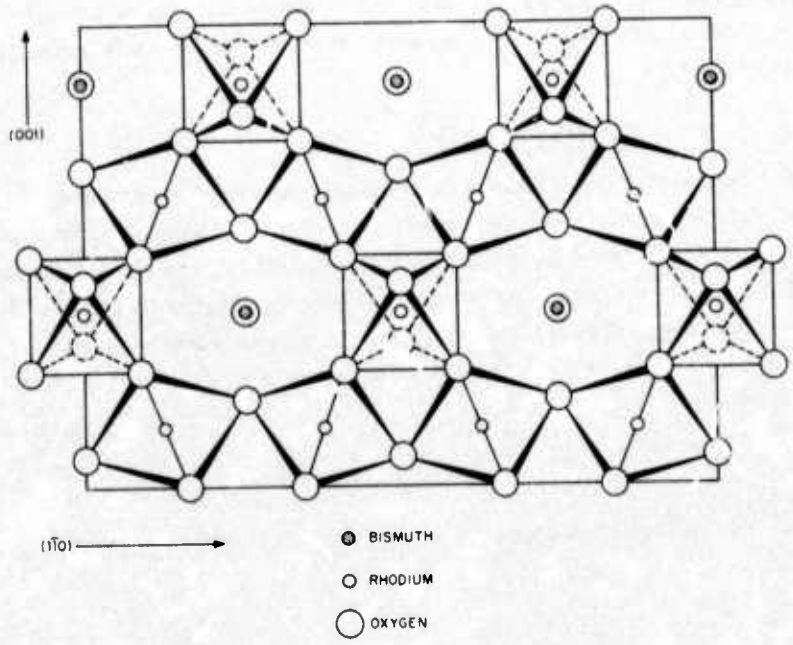

Fig. 3
The (110) projection of a cubic pyrochlore $Bi_2Rh_2O_7$ showing the (Rh_2O_6) skeleton of corner-shared octahedra and 8b-16d-8b passageways parallel to [110].

According to the simple Einstein theory for ion mobility, the conductivity is given by

$$\sigma = zNc(1-c)\, e^2 a_\ell^2 \nu / kT \qquad (1)$$

where z is the number of nearest-neighbor alkali-ion sites of density N, c is the concentration of M^+ ions on the available set of interconnected sites, e is the carrier charge, a_ℓ is the distance between sites. The jump frequency is

$$\nu = \nu_o \exp(S/k) \exp(-\delta_a/kT) \qquad (2)$$

where the Gibbs free energy for a jump is $\delta_a - TS$. The factor $c(1-c)$ defines the requirement for partial site occupancy, and the activation energy δ_a is a measure of the "bottleneck barrier" to ion transfer between equivalent lattice sites. The factor $a_\ell^2 \nu_o$ imposes the need for short jump distances, since ν_o is limited by the elastic vibrational-mode frequencies. Short-range correlation may decrease the pre-exponential factor.[6]

With these principles in mind, we have investigated four classes of skeleton structure: the Im3 phase of high-pressure $KSbO_3$, the defect-pyrochlore structure illustrated by $RbMgAlF_6$, the carnegieite structure of high-temperature $NaAlSiO_4$, and the system $Na_{1+x}Zr_2P_{3-x}Si_xO_{12}$, $0 \leqslant x \leqslant 3$.

A. The Im3 Phase

A primitive-cubic Pn3 phase of $KSbO_3$ was first discovered by Spiegelberg.[7] The structure is composed of an $(SbO_3)^-$ subarray, the skeleton, with an ordered arrangement of K^+ ions within ⟨111⟩ tunnels that traverse the skeleton, intersecting at the origin and body-center positions, see Fig. 1. The ⟨111⟩ tunnels are made up of face-shared octahedral sites that are compressed along the tunnel axis so as to provide a large spacing between the bridging O_1 and O_2 oxygen within a shared face. Along any ⟨111⟩ axis, three octahedral sites separate an origin and body-center position, and the order of the shared faces is O_1-O_2-O_2-O_1, see Fig. 2. Alkali-ion sites having O_1 and O_2 faces are labeled M_1 sites, those with only O_2 faces are M_2 sites. The unit cell contains $K_{12}Sb_{12}O_{36}$, the K^+ ions occupying the M_1 and M_2 positions in an ordered manner so that each tunnel segment contains either two M_1 cations or one M_2 cation, and an M_2 cation has only M_1-cation nearest neighbors in the neighboring tunnel segments.

The stoichiometric, atmospheric-pressure phase of $KSbO_3$ has the rhombohedral ilmenite structure. During an investigation of the structural relationships among several $A^+B^{5+}O_3$ compounds, we[8] found a cubic high-pressure phase with space group Im3. This Im3 phase has the same skeleton as the primitive-cubic Pn3 phase discovered by Spiegelberg; but it contains K^+ ions randomly distributed among the M_1 and M_2 positions.

Three characteristics of this structure are of interest: (1) Although the M_1 and M_2 sites are not crystallographically equivalent, their site-occupation energies appear to be nearly so. (2) The distance in $KSbO_3$ between M_1 and M_2 positions of a tunnel segment is only $a_{12} = 1.83$ Å, that between M_1 positions of neighboring tunnel segments is only $a_{11} = 2.66$ Å. (3) The distance from the center of an O_2 triangle to an O_2 ion is 2.5 Å, indicating that the "bottleneck" for Na^+-ion transport within a segment is not severe, and transfer between M_1 sites to neighboring tunnel segments is constrained by the crystalline fields to go through the triangular face created by an O_1-O_1 edge and the origin or body-center position. These characteristics were sufficiently promising that we decided to measure alkali-ion transport in compounds with this $(SbO_3)^-$ skeleton even though the chemical stability of the skeleton in the presence of molten alkali metals is probably not adequate for practical applications.

B. The Defect Pyrochlore AB_2X_6

The cubic pyrochlore structure corresponds to the chemical formula $A_2B_2X_6X'$, where A is a large cation and B is a smaller cation octahedrally coordinated by six X anions. The B_2X_6 subarray forms a skeleton of corner-shared octahedra, see Fig. 3. In the interpenetrating A_2X' subarray, each X' anion is tetrahedrally coordinated by four A cations, and each A cation has two nearest-neighbor X' ions on opposite sides. With space group Fd3m and the origin chosen at a B site, the A and X' positions are identified as 16d and 8b, the cubic unit cell containing $A_{16}B_{16}X_{48}X'_8$. The B and X positions are the 16c and 48f positions of the space group.

Defect pyrocholores have a stable B_2X_6 skeleton with vacancies introduced into the A_2X' subarray. In $PbRuO_3$ and $AgSbO_3$, for example, the X' atoms at the 8b sites are missing.[9,10]

Babel et al.[11] prepared a number of flourides $A^+B^{2+}B'^{3+}F_6$, where A = Cs, Rb, or K. These fluorides have a $B^{2+}B'^{3+}F_6$ skelcton identical to the B_2X_6 pyrochlore skeleton, the B and B' atoms being randomly distributed. In place of the A_2X' subarray of a pyrochlore, only the 8b positions are occupied by a large A^+ cation. In several oxides, displacement of the A cation from an 8b toward a 16d (to occupy 32e) site has been signaled.[12] Singer[13] encouraged us to explore these compounds for fast alkali-ion transport. Since the A site is a strongly squashed octahedron presenting a minimal bottleneck barrier for ion transfer between 8b and 16d positions, we decided to pursue two strategies: (1) Establish vacancies on the 8b positions by stabilizing $A^+_{1-x}B^{2+}_{1-x}B'^{3+}_{1-x}F_6$ compounds, thus making non-zero the factor $c(1-c)$ in Eq. (1) for 8b occupancy since the 16d sites are not energetically equivalent. However, this strategy suffers from a long jump distance a_{bb} between 8b positions. (2) Increase the cell size until the crystal-field preference of the M^+ ions for 16d sites balances the size preference for 8b sites, thus making the 8b and 16d positions energetically equivalent. This latter strategy seemed preferable since the jump distance a_{ab} is only half a_{bb}. Moreover, this should be the condition for minimum $\mathcal{E}_a$. This strategy was complicated by water contamination, in the case of K^+-ion transporters, and by excess Na_2O in the case of Na^+-ion transporters (see below).

C. Carnegieites

The aluminosilicates are classic skeleton structures. The zeolites, for example, form molecular sieves. As these latter structures are stabilized by water, they are unsuitable for solid electrolytes that are to be in contact with molten alkali metal. Moreover, the openings are too large for optimal alkali-ion transport. The high-temperature form of $NaAlSiO_4$, carnegieite, is a more interesting possibility.

Carnegiete has a cubic $(AlSiO_4)^-$ skeleton having the structure of cubic SiO_2, see Fig. 4. In the idealized structure, the Al and Si atoms form a cubic zinc-blende array with oxygen atoms on every Al-Si bond axis. This arrangement provides a network of corner-shared tetrahedra that, in the real carnegieite structure, becomes distorted to a primitive-cubic array by interaction with the Na^+ ions in the interstitial space.[14] In the idealized structure, the interstitial space is identical to the space occupied by the skeleton, as is well illustrated by the two interpenetrating, anticarnegieite sublattices of Cu_2O.[15] Translation of the skeleton by $a_o/2$ along a cube edge would superimpose it on the interstitial space. Thus the interstitial space has two distinguishable sites, M_1 and M_2, corresponding to the Al and Si sites of the skeleton, and any anion excess would be located on the M_1-M_2 axis in the shared face of the M_1 and M_2 sites. This face consists of a hexagon having its six sides alternately the edges of SiO_4 and AlO_4 tetrahedra. In the

absence of excess anions, which would block M^+-ion transfer, the barrier to M^+-ion motion would seem to be a minimal crystal-field energy.

D. The System $Na_{1+x}Zr_2P_{3-x}Si_xO_{12}$

From general considerations, an open skeleton allowing three-dimensional ionic transport would have skeleton anions linked to at most two skeleton cations. The stronger these skeletal bonds, the more stable the skeleton. The Im3 and defect-pyrochlore skeletons are composed of linked octahedra, the carnegieite skeleton of linked tetrahedra. A remaining alternative is a skeleton of linked tetrahedra and octahedra. To explore this possibility, we initially chose $(PO_4)^{3-}$ and $(SO_4)^{2-}$ tetrahedra to be linked by a cation with an octahedral-site preference. Since oxides of the octahedral-site cation should not be reduced by molten alkali metals, the list of suitable ions is limited. Of the quadrivalent ions, the Zr^{4+} ion was a natural candidate for the octahedral-site cation. One of us[16] preheated a mix of $Na_2CO_3 + ZrO_2 + 2NH_4H_2PO_4$ at 170°C to decompose $NH_4H_2PO_4$, again at 900°C to decompose Na_2CO_3, and heated to 1600°C for 3 hrs before turning off the furnace. Cube-shaped crystals about 0.1 mm on an edge were examined crystallographically and shown to be $NaZr_2P_3O_{12}$ with space group $R\bar{3}c$. It was also found that all the phosphor may be replaced by silicon, giving the system $Na_{1+x}Zr_2P_{3-x}Si_xO_{12}$, $0 \leqslant x \leqslant 3$. All structures are rhombohedral $R\bar{3}c$, except in the range $1.8 \leqslant x \leqslant 2.2$ where a distortion to the monoclinic C2/c space group is found at room temperature. We subsequently discovered that the structures of $NaZr_2P_3O_{12}$ and $Na_4Zr_3Si_3O_{12}$ had already been reported in the literature.[17,18]

In the $(Zr_2P_{3-x}Si_xO_{12})^{(1+x)-}$ skeleton, each Zr^{4+} octahedron shares its six corners with tetrahedra, and each tetrahedron shares its four corners with octahedra, see Ref. 16 and Figs. 5, 6. Thus each anion bonds strongly to a tetrahedral and an octahedral cation of the skeleton. In the rhombohedral phase, two M^+-ion sites are distinguishable in the interstitial space: close-packed-hexagonal M_2 layers in the basal plane connected by one-third as many M_1 sites between the M_2 layers. Thus the interstitial space is connected in three dimensions, and the anion bottleneck between M_1 and M_2 positions consists of a puckered hexagonal ring having as its six sides alternately tetrahedral-site and octahedral-site edges of the skeleton. The monoclinic distortion distinguishes two M_2 sites: $3M_2 \rightarrow M_2 + 2M_3$ as shown in Fig. 6(b). The jump distances for monoclinic $Na_3Zr_2PSi_2O_{12}$ lie in the range 3.51 – 3.8 Å.

Transport Measurements

Transport measurements were made on dense (in excess of 85 percent theoretical), polycrystalline ceramic disks approximately 1/2" in diameter and 0.05" to 0.1" thick.

Ionic conductivity was measured with an ac vector-impedance meter (5 Hz to 500 kHz). Gold or platinum blocking electrodes, which permit electron transport but restrict ionic transport to a displacement current, were used to determine any electronic component. Nonblocking electrodes, consisting of a coating of colloidal graphite on both sides of the sample, permit Na^+-ion discharge from the electrolyte, polarization at higher frequencies generally remaining trivial to frequencies as low as 500 Hz. For comparison purposes, some dc and low-frequency ac measurements were made with molten $NaNO_3$ on both sides of the specimen.

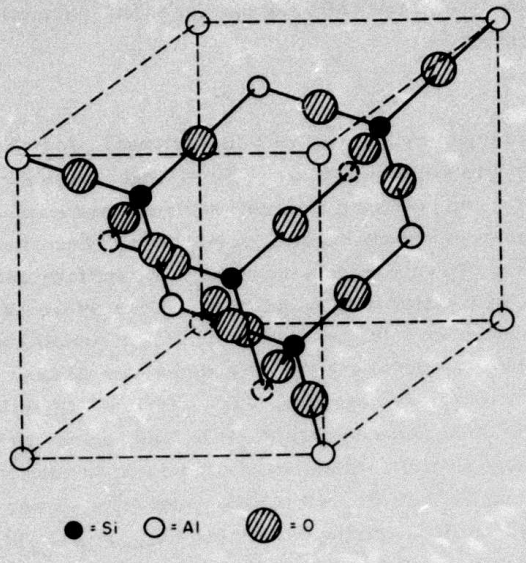

Fig. 4
The $(AlSiO_4)^-$ subarray of carnegieite.

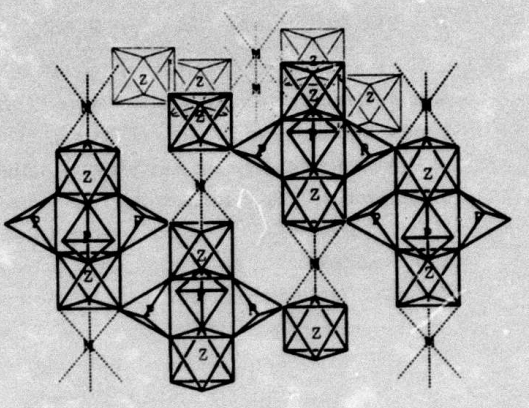

Fig. 5
View of rhombahedral $R\bar{3}c$ structure of $NaZr_2P_3O_{12}$ showing the $(Zr_2P_3O_{12})^-$ units parallel to c_r and the Na^+ ions in M_1 positions octahedrally coordinated by O^{2-} ions. The M_1 positions are also octahedrally coordinated by empty M_2 positions (not shown) in the same basal planes as the nearest-neighbor O^{2-} ions.

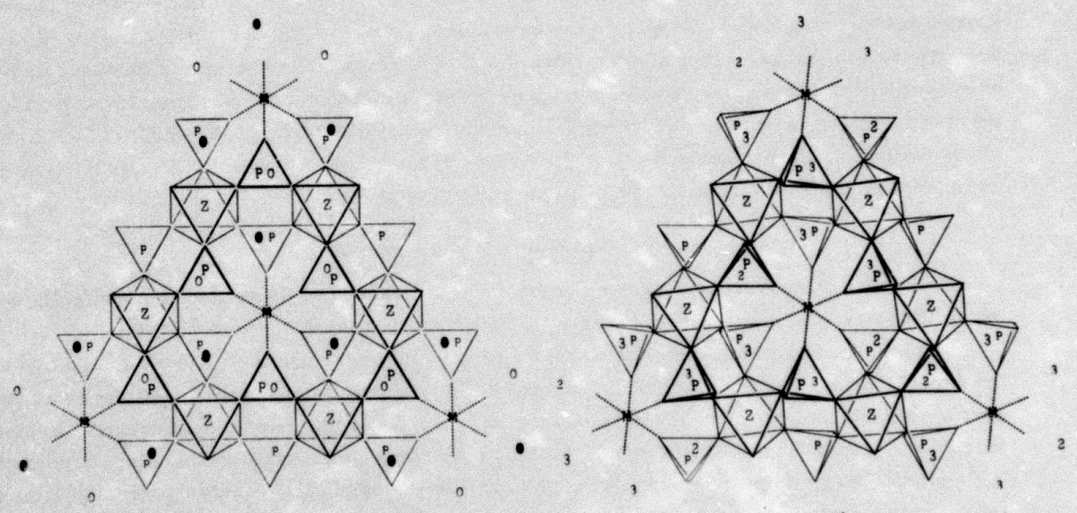

(a) $R\bar{3}c$ (b) $C2/c$

Fig. 6
Basal or a_m-b_m plane of Zr-octahedra and P-tetrahedra neighboring an M_1 site (M) showing the octahedral coordination of M_2 sites (circles).

Results

A. $NaSbO_3$

A metastable "$NaSbO_3$" phase having the cubic Im 3 structure was obtained by ion exchange, the high-pressure Im 3 phase of $KSbO_3$ or of $T\ell SbO_3$ being immersed for a few hours in molten $NaNO_3$. Single-crystal structure analysis, obtained by ion exchange of a crystal of $T\ell SbO_3$, located the Na^+ ions randomly distributed among the octahedral M_1 and M_2 sites of Fig. 2. This analysis produced three significant findings:

(1) The apparent sodium concentration is in excess of stoichiometry, suggesting a chemical formula $Na_{1+x}SbO_3$ with $x \approx 0.29$. This apparent excess could be at least partially due to an incomplete exchange of the heavier $T\ell^+$ ions, since only a single exchange bath was used.

(2) There was no measurable electron density in the tunnel intersections at the origin and body-center positions where excess O^{2-} ions were anticipated.

(3) In the disordered Im 3 phase, Na_1^+-Na_1^+ separations of only 2.30 Å apparently occur, especially as the occupancy factors of the M_1 and M_2 sites were in the ratio 0.82/0.28 rather than 2/1.

Since there was no measurable electronic component to the conductivity at 300°C, it is concluded that the ion-exchanged composition must be $NaSbO_3 \cdot yNa_2O$, $y \leqslant 0.14$, and that the excess oxygen may be displaced toward empty M_1 sites, thus blocking a fraction of the tunnel segments to Na^+-ion transport.

High pressure stabilizes the cubic Im 3 phase of $KSbO_3$ because this phase is more dense than the ilmenite $KSbO_3$. For $NaSbO_3$ the situation is reversed, which limits the pressure that can be applied for densification of the metastable, cubic $NaSbO_3$. Nevertheless, we were able to obtain specimens of 92-98 percent theoretical density by adding 2 weight percent $NaNH_2$ flux to a mixture of fine (<1 μm) powder placed in a tungsten-carbide die-and-piston assembly. After evacuation to $<10^{-3}$ Torr, a pressure of 30,000 psi was applied and the temperature was raised to 600°C for an hour or so before the pressure was released and the specimen was baked out at 500°C.

Conductivity measurements showed no measurable electronic contribution and an ionic resistivity at 300°C of $\rho_{300} = 18$ Ω-cm at 1 kHz with graphite electrodes. The fact that this resistivity is only a factor four larger than that of the best β''-alumina samples at 300°C demonstrated to us the validity of the skeleton-structure concept.

B. $NaSbO_3 \cdot \frac{1}{6}NaF$

Since the tunnel-intersection sites are empty in $NaSbO_3$, it suggests that they repel positive ions and attract negative ions. If so, the Na^+ ions jump from M_1 site to M_1 site of neighboring tunnel segments without passing through the tunnel intersections. Moreover, placement of an anion at the intersection sites could stabilize a cubic phase of $KSbO_3$, thus explaining Spiegelberg's stabilization at atmospheric pressure of the Pn3 phase by annealing for three weeks at 1000°C in a porcelain crucible. Roth[19], suspecting silicon contamination of Spiegelberg's crystal, was the first to investigate impurity stabilization of cubic $KSbO_3$. He subsequently tried stabilization of $KSbO_3$ by fluorine substitutions and reported[20] the atmospheric-pressure preparation of

Table 1: Final Atomic Parameters for $KSbO_3 \cdot 1/6KF$*

Atom	o.f.**	x	y	z	β_{11}	β_{22}	β_{33}	β_{12}	β_{13}	β_{23}
K(1) 8c	0.32(3)	1/4	1/4	1/4	0.024(4)	0.024(4)	0.024(4)	0	0	0
K(2) 16f	0.66(2)	0.1582(6)	0.1582(6)	0.1582(6)	0.0072(6)	0.0072(6)	0.0072(6)	0.0038(5)	0.0038(5)	0.0038(5)
Sb 12e		0.8421(1)	0	1/2	0.0011(1)	0.0013(1)	0.0011(1)	0	0	0
O(1) 12d		0.363(1)	0	0	0.000(1)	0.001(1)	0.005(2)	0	0	0
O(2) 24g		0	0.346(1)	0.292(1)	0.005(1)	0.002(1)	0.000(1)	0	0	0.0004(9)
F 2a		0	0	0	0.004(2)	0.004(2)	0.004(2)	0	0	0

*Number of K atoms per unit cell = 13.1 ± 0.3; Space group: Im 3; cell parameter: a = 9.606(5) Å

**Occupancy factor.

Table 2: Final Atomic Parameters for $NaSbO_3 \cdot 1/6NaF$*

Atom	o.f.**	x	y	z	β_{11}	β_{22}	β_{33}	β_{12}	β_{13}	β_{23}
Na(1) 8c	0.25(4)	1/4	1/4	1/4	0.009(4)	0.009(4)	0.009(4)	0	0	0
Na(2) 16f	0.80(4)	0.154(1)	0.154(1)	0.154(1)	0.024(2)	0.024(2)	0.024(2)	0.004(1)	0.004(1)	0.004(1)
Sb 12e		0.8381(1)	0	1/2	0.0032(1)	0.0037(1)	0.0033(1)	0	0	0
O(1) 12d		0.360(1)	0	0	0.000(1)	0.006(1)	0.005(1)	0	0	0
O(2) 24g		0	0.3325(9)	0.2873(9)	0.006(1)	0.003(1)	0.005(1)	0	0	0.0003(9)
F 2a		0		0	0.004(1)	0.004(1)	0.024(1)	0	0	0

*Number of Na atoms per unit cell = 14.7 ± 0.6; Space group: Im 3; cell parameter: a = 9.306(1) Å

**Occupancy factor.

$K_{1-x}SbO_{3-x}F_x$. Since he failed to report any chemical analysis, it is probable that his phase was $KSbO_3 \cdot xKF$, $0 < x \leq 1/6$. We independently investigated the atmospheric-pressure phase $KSbO_3 \cdot 1/6KF$, since we were interested not only in the possibility of eliminating a high-pressure step in the preparation of $NaSbO_3 \cdot 1/6NaF$, but also in whether the existence of an anion at the tunnel intersections would aid or hinder Na^+-ion mobility.

The precursor $KSbO_3 \cdot 1/6KF$ was prepared by firing a 2:1 by-weight mixture of $K_2H_2Sb_2O_7 \cdot 4H_2O$:KF at 900°C for 2 hours. A cubic product was separated from the excess KF by washing in water. This product was ion-exchanged three successive times with $NaNO_3$ at 330°C in a 20:1 by-weight mixture of $NaNO_3$:product. The triple-ion-exchanged product, which remained cubic, was hot-pressed into disks for ion-transport measurements.

In order to characterize the products with single-crystal structure analysis, a mixture of 20 g potassium pyro-antimonate and 100 g KF was fired in a covered platinum crucible at 1100°C for 12 hours and then programmed down at a rate of 5°C/hour to room temperature. Many well shaped single crystals about 0.05 mm in size were obtained. Powder diffraction of the specimen showed a body-centered-cubic pattern. A crystal measuring 0.03 × 0.03 × 0.05 mm was selected for structural analysis. The sodium analog was prepared by ion exchange in molten $NaNO_3$. The sodium crystal selected for structural analysis measured about the same size as that of the potassium analog.

Oscillation and Weissenberg photographs of both crystals showed diffraction symmetry m3. The systematic absence was $hk\ell$ for $h + k + \ell = 2n + 1$, which is consistent with space groups I23, $I2_13$, and Im 3. The space group Im 3 was assigned as determined for the Im 3-$NaSbO_3$ structure.[8] Three-dimensional intensity data to $2\theta = 55°$ were collected in the same fashion as in Ref. 8. A total of 605 reflections was measured for the $KSbO_3$-KF product, 498 for the sodium analog.

A strong similarity between the powder patterns of Im 3-$NaSbO_3$ and the new phase induced us to use an identical $(SbO_3)^-$ skeleton for the initial refinement. The least-squares program gave a reliability factor R = 0.17 for the $KSbO_3 \cdot KF$ product, R = 0.14 for the ion-exchanged crystal. From the calculated structure factors based on this model, a difference Fourier map in both cases revealed two independent alkali-ion positions at (x, x, x): a larger electron density at x = 0.15 and a lower at x = 1/4. Unlike the Im 3-$NaSbO_3$ pattern, a considerable electron density appeared at (0, 0, 0), or the tunnel-intersection sites 2a. We assigned F^- ions to the 2a site in both cases, corresponding to compositional formulas $KSbO_3 \cdot 1/6KF$ and $NaSbO_3 \cdot 1/6NaF$, and obtained reliability factors R = 0.077 and R = 0.064, respectively, after a few refinement cycles with anisotropic temperature factors. The final analyses are summarized in Tables 1-3.

Comparison of the Im 3-$NaSbO_3$ and the $NaSbO_3 \cdot 1/6NaF$ structures is instructive. The Im 3-$NaSbO_3$ product of ion exchange with cubic $KSbO_3$ or $TlSbO_3$ contains excess electron density, presumably indicating $NaSbO_3 \cdot xNa_2O$. The apparent occupancies of the sodium-atom sites are 29 percent at 8c (M_2) and 82 percent of 16f (M_1); the tunnel-intersection sites 2a are empty. The 16f positions form a simple cube about each 2a site, and the shortest 16f-16f ($M_1 - M_1$) separation is only 2.27 Å in Im 3-$NaSbO_3$. This surprisingly short distance seems to imply the displacement of the excess O^{2-} ions toward vacant 16f positions. In the $NaSbO_3 \cdot 1/6NaF$ structure, on the other hand, each 2a site is occupied by an F^- ion and there is no apparent sodium-atom excess over the chemical formula. The sodium-atom site occupancies are 25 percent at 8c and 80 percent at 16f, and the shortest Na^+-Na^+ distance is 2.85 Å.

Table 3: Bond Distances (in Å) in $KSbO_3 \cdot 1/6KF$ and $NaSbO_3 \cdot 1/6NaF$

		$KSbO_3 \cdot 1/6KF$	$NaSbO_3 \cdot 1/6NaF$
Octahedron around Sb			
Sb – O(1)	2x	2.008(6)	1.994(6)
– O(2)	2x	1.960(9)	1.947(8)
	2x	1.995(9)	1.979(8)
Octahedron around alkali ion M(1)			
M(1) – O(2)	6x	2.604(4)	2.474(3)
Octahedron around alkali ion M(2)			
M(2) – O(1)	3x	2.913(6)	2.79(1)
– O(2)	3x	2.686(9)	2.52(1)
Cube around F			
F – M(2)	8x	2.632(6)	2.482(9)

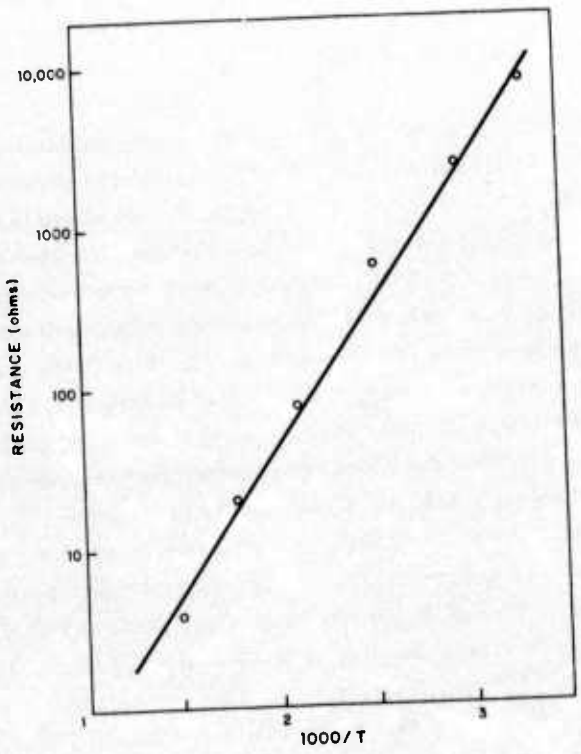

Fig. 7
Resistance vs 1/T for a typical ceramic specimen of $NaSbO_3 \cdot NaF$ with graphite electrodes at 1 kHz.

An anomalously high temperature coefficient is observed for the Na^+ ions in positions 16f, the anisotropic temperature coefficient indicating that the thermal motion along cubic axes is six times larger than that along cubic diagonals. Isostructural $KSbO_3 \cdot 1/6KF$, which also contains no M^+-ion excess, has a temperature coefficient only one-third as large. These findings are consistent with higher Na^+-ion mobility in $NaSbO_3 \cdot 1/6NaF$ and with a hopping of Na^+ ions between 16f positions of different tunnels that not only is around the 2a sites, but also is easier than hopping within a tunnel segment.

Although $NaSbO_3 \cdot 1/6NaF$ has moderate temperature stability, it cannot be heated to temperatures near the melting point and it cannot sustain very high pressures. At 5000 atmospheres and 600°C, there is a partial disproportionation and transformation to the more dense ilmenite phase of $NaSbO_3$. Therefore, hot-pressed disks for ion-transport measurements were prepared in the same manner as the $NaSbO_3$ disks. Samples of 92-percent density had 1-kHz resistivities at 300°C of $\rho_{300} = 13$ and 17 Ω-cm, respectively, for measurements made with graphite and molten $NaNO_3$ electrodes. With d.c. and molten $NaNO_3$ electrodes, a $\rho_{300} = 18$ Ω-cm was obtained. Fig. 7 shows a plot of resistance vs 1/T for a typical specimen of $NaSbO_3 \cdot 1/6NaF$. The slope yields an activation energy of $\mathcal{E}_a \approx 0.35$ eV for a Na^+-ion jump.

From these measurements we deduce three conclusions: (1) Cubic skeleton structures have the improvement in pre-exponential factor of Eqs. (1) and (2) anticipated for bulk vs layer Na^+-ion conduction. (2) Placement of an anion at the tunnel intersections does not impede the Na^+-ion mobility, thereby confirming that the Na^+ ions avoid these positions in cubic $NaSbO_3$. (3) Reduction in the Na^+-ion activation energy $\mathcal{E}_a$ for hopping would make the transport properties of cubic skeleton structures superior to those of β-alumina.

In order to determine how $\mathcal{E}_a$ changes with lattice parameter, we attempted to study the Na^+-ion conductivity as a function of pressure. Unfortunately the die broke before we could obtain quantitative data, but the data clearly indicated that the conductivity decreases with the lattice parameter ($d\sigma/da_o > 0$). Since the pre-exponential factor should be relatively pressure-insensitive, we may conclude that a smaller $\mathcal{E}_a$ can be achieved by increasing the lattice parameter a. We have found that isostructural $KBiO_3$ is hygroscopic, but it would be interesting to explore the system $NaSb_{1-x}Bi_xO_3 \cdot 1/6NaF$ to see how $\mathcal{E}_a$ changes with cell size for those compositions where H_2O contamination is not a problem. Since our objective was a practical electrolyte stable against molten sodium, we did not pursue this investigation.

C. Defect Pyrochlore

Initially we prepared the defect pyrochlore "$KTaWO_6$" by conventional ceramic techniques. A nominal "$NaTaWO_6$" was prepared by ion exchange in molten $NaNO_3$. At 300°C, the resistivity of this compound was about a factor 10 larger than that of $NaSbO_3 \cdot 1/6NaF$, but a lower activation energy made it interesting. Because W^{6+} ions would be reduced to W^{5+} ions by molten sodium, we turned to a study of the chemically more stable pyrochlore $A^+Ta_2O_5F$. In the course of this study, we found that the pyrochlores may be hydrated, and a subsequent investigation of nominal $NaTaWO_6$ showed it to be, in fact, partially hydrated at room temperature: $NaTaWO_6 \cdot xH_2O$ with $x \approx 0.5$.

The compound $RbTa_2O_5F$ can be synthesized directly. Equal amounts of dry RbF and reagent-grade Ta_2O_5 were mixed in a crucible and fired at 750°C under an argon atmosphere for two days. Regrinding and refiring two times produced single-phase powders. Single crystals of $RbTa_2O_5F$ were prepared by addition of excess RbF as a flux. In one run, a 4:1 ratio of

RbF and Ta_2O_5 was fired at 1150°C for 30 minutes and quenched. The product contained crystals about 0.1 mm across.

The K and Na analogs could be synthesized directly. If $RbTa_2O_5F$ is placed in molten KNO_3, the ion-exchange product is KTa_2O_5F. Chemical analysis gave Rb:Ta and K:Ta ratios of 1:2, even on reversing the exchange. On exposure to air KTa_2O_5F becomes hydrated to $KTa_2O_5F \cdot H_2O$. The lattice parameter of $RbTa_2O_5F$ is 10.496 Å, of $KTa_2O_5F \cdot H_2O$ is 10.605 Å. TGA measurements showed a reversible, broad transition from 50° to 200°C having a weight loss of one H_2O molecule per KTa_2O_5F molecule. Ion exchange from $RbTa_2O_5F$ with molten $NaNO_3$ did not yield the completely exchanged product $NaTa_2O_5F$. It was necessary to ion exchange first with K^+ ions and then with Na^+ ions. Chemical analysis gave a Na:Ta ratio of x:2 where $1 < x < 3$.

In order to determine the ionic distribution over the interstitial 16d and 8b sites, single crystals were selected for structure analysis. Oscillation and Weissenberg photographs showed diffraction symmetry m3m for the products of both potassium and sodium exchange. The systematic absence was hk0 for $h + k = 4n + 1$, which is consistent with the space group Fd3m reported for the pyrochlores. Moreover, an additional absence occurs wherever the hk*l* are all even and the index is not 4n, indicating that position 32e of Fd3m cannot be occupied. Thus, as in the normal pyrochlore structure, the $X_6 = O_5F$ atoms are randomly distributed over the 48f sites, and the B = Ta atoms occupy the 16c sites of the BX_3 skeleton. To determine the alkali-ion distribution over the 16d and 8b sites, three-dimensional intensity data to $2\theta = 60°$ were collected and analyzed as described in Ref. 8. Table 4 summarizes the results of the structural refinements.

In $RbTa_2O_5F$, the 8b sites are completely occupied by Rb atoms and the 16d sites are empty. The 8b site has 6 nearest-neighbor X atoms that form an ideal octahedron and 12 next-nearest-neighbor X atoms. The Rb-X distances are 3.35 Å and 3.78 Å, respectively. A lack of electron density at the 16d sites is consistent with the short distance, only 2.27 Å from 8b to 16d.

In $KTa_2O_5F \cdot H_2O$, x-ray data show electron density at both the 16d and 8b sites in ratio 2.5:1. There are two possible explanations: (1) K^+ ions are randomly distributed over 16d and 8b sites, or (2) K^+ ions occupy half the 16d sites and water occupies the 8b sites. Since the O^{2-} ion has an 8b-site preference and since just one H_2O molecule is accepted per molecule, the latter alternative can be inferred. Therefore, we conclude that the large cell size for the K analog corresponds to the hydrated compound $KTa_2O_5F \cdot H_2O$, the water occupying the 8b sites, even though the distance 2.29 Å between 8b and 16d sites gives a surprisingly short K-O separation.

Whereas chemical analysis of the sodium analog gave a Na:Ta ratio x:2, with $x \approx 2$, Table 4 gives an apparent Na^+-ion excess equivalent to $x \approx 3$. We thought this discrepancy might be due to the presence of OH^- ions giving $Na_2Ta_2O_5F \cdot OH$, but neither IR data nor TGA experiments nor the preparation of "$NaTa_2O_5F$" from anhydrous KTa_2O_5F gave any evidence of the presence of OH^- ions. Since electrical measurements gave no measurable electronic component to the conductivity, we concluded that the excess sodium is charge-compensated by O^{2-} ions. Anion analysis (by vacuum fusion at MIT) of a sample having a Na:Ta ratio x:2, with $x \approx 1.55$, gave $Na_{1.55}Ta_2O_{5.28}F$, corresponding to $NaTa_2O_5F \cdot 0.28\ Na_2O$. The excess O^{2-} ions presumably occupy 8b positions. X-ray intensities indicate that some Na^+ ions also occupy the 8b sites.

Excess Na_2O appears characteristic of many fast Na^+-ion conductors, including $(1 + x)\ Na_2O \cdot 11Al_2O_3$. In $NaTa_2O_5F \cdot xNa_2O$, the amount of excess Na_2O and the lattice

Table 4: Final Atomic Parameters for MTa_2O_5F (M = Rb, K, Na_x)

	$RbTa_2O_5F$	KTa_2O_5F	$Na_xTa_2O_5F$
Cell size a (Å)	10.496(3)	10.605(3)	10.470(2)
48f x	0.306(2)	0.305(2)	0.308(1)
†	0.1(4)	0.6(4)	1.8(2)
16d o	0	0.5	0.96(5)
†		17(3)	5.1(6)
16c †	0.65(6)	0.98(6)	1.08(2)
8b o	1	H_2O	1.05(7)
†	5.4(5)	15(6)	5.7(8)
R	0.10	0.10	0.053

x = position parameter of O_5F o = occupancy factor

† = isotropic temperature factor R = discrepancy factor

Table 5: Lattice Parameters and Hydration of Defect Pyrochlore AB_2X_6

1. A = Li, Na, Ag and B = Nb, Sb, Ta: $ABWO_6 \cdot H_2O$ with $10.27 \leqslant a \leqslant 10.42$ Å

2. A = K:

$KMgAlF_6$	$KNiAlF_6$	$KCuCrF_6$	$KSbWO_6$	$KNbWO_6$	$KTaWO_6$
9.86	9.92	monocl.	10.23	10.33	10.34

$KNiCrF_6 \cdot H_2O$	$KCoCrF_6 \cdot H_2O$	$KTaWO_6 \cdot H_2O$	$KNbWO_6 \cdot H_2O$
10.45	10.48	10.48	10.50

$KNiVF_6 \cdot H_2O$	$KTa_2O_5F \cdot H_2O$
10.51	10.61

3. A = Rb, Tl, Cs: All AB_2X_6 with $9.94 \leqslant a_o \leqslant 10.57$ Å

parameter are found to vary with the temperature and duration of the ion-exchange process, giving $10.44 < a_o < 10.48$ Å. Similar results were obtained when molten $NaCO_3$ was used for the ion exchange. The potential for oxidation was not even avoided by exchanging with $NaNH_2$, since it melts at a lower temperature where the $KTa_2O_5F \cdot H_2O$ is hydrated.

Preparation of hot-pressed, ceramic disks of the sodium compound is complicated by the fact that both temperature and pressure induce disproportionation to TaO_2F and the perovskite $NaTaO_3$. Specimens approaching 82 percent theoretical density were prepared by the procedures used to make pellets of $NaSbO_3$. A $\rho_{300} \approx 150$ Ω-cm and an $\delta_a \approx 0.4$ eV were obtained with graphite electrodes and 1 kHz. This finding is compatible with 16d sites partially occupied by Na^+ ions. Slight differences in ρ_{300} and δ_a were observed from sample to sample, but no correlation of the transport properties with a_o was attempted.

Table 5 lists known defect pyrochlores of the type AB_2X_6 and their lattice parameters. The Rb^+, Tl^+, and Cs^+ compounds, which have A^+ ions only in 8b sites (though perhaps displaced from the center), are dehydrated. The K^+ compounds, on the other hand, are only dehydrated if the lattice parameter is small enough to retain the K^+ ions in 8b sites. Compounds with larger lattice parameter become hydrated on exposure to air. These findings suggest there is a critical lattice parameter for hydration that is smaller than, but near the parameter at which K^+ ions have equal preference for 8b and 16d sites. Defect pyrochlores with small A^+ ions (Li^+, Na^+, Ag^+) are all either hydrated[21] or contain excess A_2O, the A^+ ions occupying 16d sites.

Ion exchange of $RbMgAlF_6$, a = 9.94 Å, gives anhydrous $KMgAlF_6$ with a = 9.86 Å and a noncubic "$NaMgAlF_6$" that can be reverse ion exchanged. Location of the K^+ ions on 8b sites was not independently confirmed by single-crystal structure analysis, but it can be inferred. Unlike the MTa_2O_5F system, these materials hot-press readily. After a preliminary bake at 200°C, vacuum pressing at 60,000 psi at 500°C for one hour yielded disks of over 99-percent theoretical density. The ionic conductivity of $KMgAlF_6$ is extremely low ($\rho_{300} = 20{,}000$ Ω-cm), presumably because the 8b array is filled. In this case, transfer of a K^+ ion to a neighboring 16d position costs a large K^+-K^+ electrostatic energy, since each 16d position has two near-neighbor 8b positions at a distance of only 2.12 Å. Therefore, we introduced cation vacancies at the 8b positions by preparing samples with chemical formula $K_{1-x}Mg_{1-x}Al_{1+x}F_6$, x = 0.05 and 0.10. The pyrochlore structure was unstable for $x > 0.1$. Cation vacancies at 8b positions would permit K^+-ion transfer from one 8b site to another via the 16d intermediary position. A dramatic increase in conductivity was observed. A plot of K^+-ion conductivity vs reciprocal temperature for a $K_{0.9}Mg_{0.9}Al_{1.1}F_6$ disk over 99-percent dense gave $\rho_{300} \approx 800$ Ω-cm and an $\delta_a \approx 0.35$ eV.

From these experiments we draw the following conclusions: (1) The B_2X_6 network of the $A_2B_2X_6X'$ pyrochlore structure is a suitable skeleton for fast ion transport. (2) Direct preparation of anhydrous defect-pyrochlore $A^+B_2X_6$ requires large A^+ cations (Cs^+, Rb^+, and – for lattice parameters below a critical size – K^+ ions) that are stabilized in the 8b (or X') positions. (3) Fast ion transport of the K^+ ions among the 8b sites requires the introduction of 8b-site vacancies, as in $K_{0.9}Mg_{0.9}Al_{1.1}F_6$. (4) Indirect preparation of defect pyrochlores $A^+B_2X_6$ having smaller A^+ cations randomly distributed on 16d sites is plagued by the introduction on 8b sites of water or of excess anions. We failed to obtain a "clean" $A^+B_2X_6$ pyrochlore having A^+ ions randomly distributed on 16d positions. However, Na^+-ion transport in partially filled 16d positions occurs in $NaTa_2O_5F \cdot xNa_2O$. It would be interesting to compare the conducitivity in this compound with that in a compound like $NaW_2O_6 \cdot F$, if such a defect pyrochlore can be prepared.

Although these results indicate that the defect-pyrochlore structure is capable of providing fast alkali-ion transport, an activation energy of 0.35 eV is still a factor two higher than desired. Therefore, we turned to other skeleton structures.

D. Carnegieite Skeletons

Because cubic $NaAlSiO_4$ is unstable at room temperature, we prepared the related stable compound $NaAlSiO_4 \cdot xNa_2O$, with x = 0.25 and 0.5, and $Na_{1+y}Mg_yAl_{1-y}SiO_4$ with y = 5/8. A ceramic disk was made from the first of these by adding NaF as a binder and H_2O to form a slurry. The mixture was vacuum-baked at 150°C and then vacuum-fired under 15,000 psi at 950°C. The resulting disk had a density of the order of 75 percent and a resistivity ρ_{300} = 1900 Ω-cm. The second was "melted" in a crucible to form a disk-shaped lump filled with bubbles. Our suspicion that some form of decomposition occurred is supported by the measured resistivity ρ_{300} = 600 Ω-cm, since the nominal amount of sodium should have filled all the available sodium positions. The third material was pressed into a disk by firing at 820°C in air under 20,000 psi. It had a ρ_{300} = 200 Ω-cm. Although ρ_{300} is more than an order of magnitude higher than that of $NaSbO_3 \cdot 1/6NaF$, it nevertheless indicates that the carnegieite skeleton may yield solid electrolytes of practical interest.

E. The System $Na_{1+x}Zr_2P_{3-x}Si_xO_{12}$

In order to obtain dense ceramic disks of compositions in the system $Na_{1+x}Zr_2Si_xP_{3-x}O_{12}$, appropriate mixtures of Na_2CO_3, Zr_2, SiO_2, and $NH_4H_2PO_4$ were heated for 16 hours at 170°C (to decompose the $NH_4H_2PO_4$) and calcined at 900°C for 4 hours. The product was cold-pressed at 80,000 psi after the addition of 4-percent polyethylene glycol as a binder. The cold-pressed pellets were fired for 6 to 16 hours at temperatures between 1200 and 1400°C. The firing temperature of $Na_3Zr_2PSi_2O_{12}$, for example, was 1250°C, since at 1275°C there was appreciable decomposition of the specimen. Densities as high as 94 percent were obtained with this method. Transport measurements with blocking electrodes indicated a negligible electronic contribution, and prolonged immersion in molten sodium showed chemical stability to this environment. Table 6 lists the resistivities at 300°C for Na^+-ion transport as obtained with graphite electrodes at 1 kHz on ceramic disks more than 85-percent theoretical density. Fig. 8 shows a plot of T/R vs 1/T, where R is the sample resistance, for a ceramic disk of $Na_3Zr_2PSi_2O_{12}$. The activation energy obtained from this plot is $\mathcal{E}_a$ = 0.29 eV.

The compound $NaZr_2P_3O_{12}$ has all the M_1 sites occupied by Na^+ ions, none of the M_2 sites.[16] Since the M_1 and M_2 sites are not energetically equivalent, the factor c(1 − c) approaches zero in Eq. (1), and the resistivity of this compound is very high. Substitution of Si for P is charge compensated by the introduction of Na^+ ions on M_2 sites, which are linked to one another via M_1 sites. Therefore, so long as the M_1 sites remain occupied, Na^+-ion conductivity requires a correlated ionic motion: $Na_2^+ + Na_1^+ + \square_2 \rightarrow \square_2 + Na_1^+ + Na_2^+$, where the subscripts refer to sites M_1 and M_2 and □ represents an empty site. The fact that the lowest values of ρ_{300} occur where the rhombohedral axis c_r and cell volume are a maximum[16] suggests that Na^+-Na^+ electrostatic interactions reduce the M_1-site preference energy with increasing x. For x > 2, both M_1 and M_2 vacancies must coexist at 300°C. The fact that the crystal-cell volume reaches a maximum with increasing x suggests that the electrostatic forces between Na^+ ions at adjacent M_1 and M_2 sites may actually displace Na^+ ions toward bottleneck positions between M_1 and M_2 sites.

Table 6: Resistivities at 300°C and Activation Energies (σT vs T^{-1}) of Dense (>85% Theoretical) Ceramic Specimens in the System $Na_{1+x}Zr_2P_{3-x}Si_xO_{12}$ with Graphite Electrodes at 500 kHz*

Composition (x)	Structure	ρ_{300} (Ω-cm)	δ_a (eV)
0.4	R	1867	0.26
0.8	R	341	0.31
1.2	R	38	0.27
1.6	R	21	0.32
1.8	M	8	0.24
2.0	M	5	0.29
2.2	M	6	0.24
2.4	R	9	0.26
2.6	R	28	0.24
2.8	R	56	0.24

*σ(500 kHz)/σ(10 kHz) ≈ 2. Higher frequencies used to reduce electrode polarization.

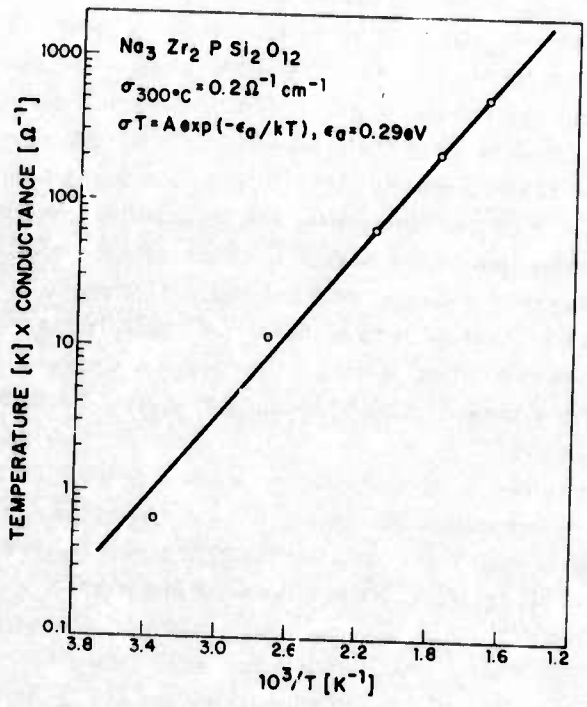

Fig. 8
Temperature – conductance product T/R vs 1/T for a typical ceramic specimen of $Na_3Zr_2PSi_2O_{12}$ with graphite electrodes at 500 kHz.

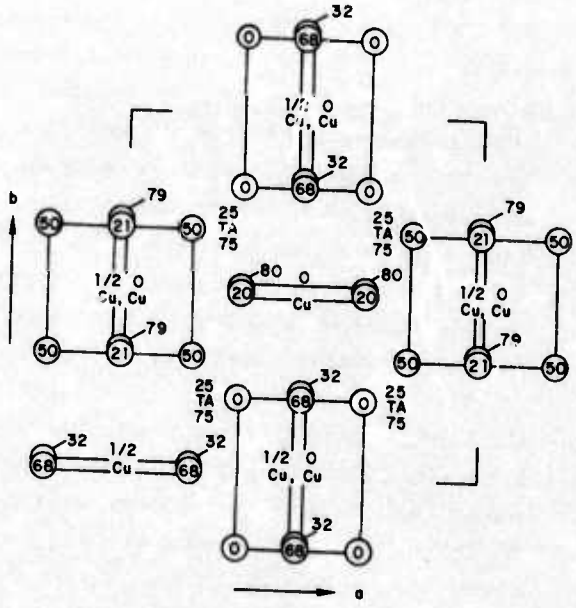

Fig. 9
Structure of $CuTa_2O_6$ showing orientations of the Square CuO_4 units.

At 300°C, the transport properties of $Na_3Zr_2PSi_2O_{12}$ are clearly equivalent to those of β''-alumina at temperatures T > 300°C, but inferior for T < 300°C. A much improved pre-exponential factor is consistent with the three-dimensional character of the Na^+-ion transport in $Na_3Zr_2PSi_2O_{12}$. The fact that β''-alumina has an activation energy 0.1 eV smaller than that of $Na_3Zr_2PSi_2O_{12}$ leaves hope that three-dimensional Na^+-ion transport in skeleton structures may also have activation energies as low as 0.2 eV. With the improved pre-exponential factor of three-dimensional transport, such Na^+-ion conductors would be competitive with liquid electrolytes at room temperature.

The system $Na_{1+x}Zr_2P_{3-x}Si_xO_{12}$ appears to be easier to fabricate into dense ceramics than β''-alumina. We have made both open and closed-ended tubes of $Na_3Zr_2PSi_2O_{12}$ at 90-percent theoretical density with preliminary extrusion/isostatic-pressing techniques.

The system $Na_{1+x}Zr_2P_{3-x}Si_xO_{12}$ is only one representative of a large class of compounds that can be stabilized with this basic structure. Ion exchange with Li^+, Ag^+, and K^+ ions has been successfully accomplished.[16] Other ions can replace the octahedral Zr^{4+} ions. However, we were not able to replace Si by Ge, which is suggestive of a size constraint for the tetrahedral ion.

We would like to thank J. Singer for helpful discussion, K. Dwight for Figs. 5 and 6, Carl Anderson and David Tracy for technical assistance.

APPENDIX

The defect perovskite $CuTa_2O_6$ has a $(TaO_3)^-$ skeleton of corner-shared octahedra, but it is strongly distorted from the cubic ReO_3 structure.[22] Reinen and Propach[23] independently deduced the Pm 3 space group on the basis of optical and powder-diffraction data, but they did not determine the atomic positions. Single-crystal structure analysis[22] confirmed the existence of square-coplanar oxygen coordination about Cu^{2+} ions and located them at positions 3d and 3c. Although it is remarkable that so small a cation as Cu^{2+} should occupy the A site of a perovskite, this is made possible by the distortion of the TaO_3 network that reduces the A-site anion coordination from twelve to four nearest neighbors.

Fast Na^+-ion transport is not found in cubic perovskite, presumably because the (oxygen-square) bottlenecks at the shared Na-site faces have too small an area. However, the Cu^{2+} ion should be small enough to pass through such a bottleneck. Moreover, the distortion of the $(TaO_3)^-$ skeleton creates square-coplanar configurations at 3/4 of the cubic-perovskite A sites, see Fig. 9, and the Cu^{2+} ions are randomly distributed over these square-coplanar sites, which are 2/3-filled in $CuTa_2O_6$. However, the orientations of the square complexes are such that a Cu^{2+} ion must pass through an edge of the square on jumping from site to site.

Powder samples are green. Single crystals grown from a copper-oxide flux are dark. Conductivity measurements on single-crystal specimens with copper electrodes gave an $\mathcal{E}_a$ = 0.36 eV, obtained from σT vs T^{-1}, and a $\rho_{300} \approx 1000$ Ω-cm. With gold or platinum electrodes the resistivity at 300°C was a factor of 10 larger. We conclude that our single-crystal conductivity was mixed, but that the Cu^{2+}-ion conduction dominated.

REFERENCES

1. Y. F. Yao and J. T. Kummer J. Inorg. Nucl. Chem. 29, 2453 (1967); J. T. Kummer and N. Weber Proc. 21st Ann. Power Sources Conf. (1967) and M. S. Patent 3,404,035 (1968).
2. J. T. Kummer and N. Weber, U.S. Patent No. 3,475,223.
3. M. S. Whittingham and R. A. Huggins, NBS Special Publication 364, R. S. Roth and S. J. Schneider, Jr., eds. (July 1972), p. 139; A. V. Virkar, G. J. Tennenhouse, and R. S. Gordon, J. Am. Ceram. Soc. 57, 508 (1974).
4. R. S. Gordon, NSF Program Review, Dearborn, Mich. (Jan. 30, 1975).
5. R. Ridgeway, A. Klein, and W. O'Leary, Trans . Electrochem. Soc. 70, 71 (1936).
6. D. B. McWhan, S. J. Allen, Jr., J. P. Remeika, and P. D. Dernier, Phys. Rev. Letters 35, 953 (1975).
7. P. Spiegelberg, Ark. Kemi 14A, 1 (1940).
8. J. A. Kafalas, NBS Special Publication 364, R. S. Roth and S. J. Schneider, Jr., eds. (July 1972), p. 287; H. Y-P. Hong, J. A. Kafalas, and J. B. Goodenough, J. Solid State Chem. 9, 345 (1974).
9. J. M. Longo, P. M. Raccah, and J. B. Goodenough, Mater. Res. Bulletin 4, 191 (1969).
10. N. Schrewelius, Z. Anorg. Allgem. Chem. 238, 241 (1938).
11. D. Babel, G. Pausewang, and W. Viebahn, Z. Naturforsch. 22b, 1219 (1967).
12. C. Michel, D. Groult, and B. Raveau, Mat. Res. Bull. 8, 201 (1973); J. L. Fourquet, C. Jacobini, and R. de Pape, Mat, Res. Bull. 8, 393 (1973).
13. J. Singer, contract monitor.
14. W. Borchert and J. Keidel, Heidelberg Beitr. Mineral, u Petrogr. 1, 17 (1947).
15. L. Pauling, The Nature of the Chemical Bond, 3rd Ed, Cornell Univ. Press (1960), p. 254.
16. H. Y-P. Hong, companion paper.
17. L. Hagman and P. Kierkegaard, Acta Chem. Scand. 22, 1822 (1968).
18. R. G. Sizova, A. A. Voronkov, N. G. Shumyatskaga, V. V. Pynkhin, and N. V. Belov, Dokl. Akad, Nauk SSSR, Ser. 205, Issue 1, 90 (1972).
19. R. S. Roth, H. S. Parker, W. S. Brower, and D. Miner, NASA Contract C-50821-C Final Report, CR-134869 (July 1975).
20. W. S. Brower, D. B. Minor, H. S. Parker, and R. S. Roth, Mater. Res. Bulletin 9, 1045 (1974).
21. C. Michel, D. Groult, and B. Raveau, J. Inorg. Nucl. Chem. 37, 247 (1975).
22. H. Y-P. Hong, Lincoln Laboratory, M.I.T., Solid State Research Report (1972:2), p. 33.
23. D. Reinen and V. Propach, Inorg. Nucl. Chem. Letters 7, 569 (1971).

III. PAPER TO APPEAR FEBRUARY ISSUE OF MATERIALS RESEARCH BULLETIN

CRYSTAL STRUCTURES AND CRYSTAL CHEMISTRY IN THE SYSTEM $Na_{1+x}Zr_2Si_xP_{3-x}O_{12}$*

H. Y-P. Hong
Lincoln Laboratory, Massachusetts Institute of Technology
Lexington, Massachusetts 02173

ABSTRACT

As part of a search for skeleton structures for fast alkali-ion transport, the system $Na_{1+x}Zr_2Si_xP_{3-x}O_{12}$ has been prepared, analyzed structurally and ion exchanged reversibly with Li^+, Ag^+, and K^+ ions. Single-crystal x-ray analysis was used to identify the composition $NaZr_2P_3O_{12}$ and to refine its structure, which has rhombohedral space group $R\bar{3}c$ with cell parameters $a_r = 8.815(1)$ Å. A small distortion to monoclinic symmetry occurs in the interval $1.8 \leq x \leq 2.2$. The structure for $Na_3Zr_2Si_2PO_{12}$, proposed from powder data, has space group C2/c with $a_m = 15.586(9)$ Å, $b_m = 9.029(4)$ Å, $c_m = 9.205(5)$ Å, and $\beta = 123.70(5)°$. Both structures contain a rigid, three-dimensional network of PO_4 or (SiO_4) tetrahedra sharing corners with ZrO_6 octahedra and a three-dimensionally linked intersitial space. Of the two distinguishable alkali-ion sites in the rhombohedral structure, one is completely occupied in both end members, the occupancy of the other varies across the system from 0 to 100 percent. Several properties are compared with the fast Na^+-ion conductor β-alumina.

Introduction

The research reported here was motivated by active interest in solid electrolytes having fast alkali-ion transport and by the proposition (1) that solid electrolytes having alkali-ion conductivities approaching those of liquids should occur in skeleton structures. Potential skeleton structures would consist of a rigid, three-dimensional network stabilized by electrons donated by transporting ions partially occupying a three-dimensionally linked interstitial space. Moreover, the smallest cross-sectional areas of an interstitial passageway, designated "bottlenecks" (2), should have smallest diameters greater than twice the sum of the anion and alkali-ion radii. For Na^+-ion transport in an oxide, the bottleneck smallest diameter should, therefore, exceed 4.8 Å.

In addition to these geometrical constraints, chemical bonding also plays a role. If the crystalline fields and/or the site binding energy preferentially stabilizes an alkali ion at a particular set of lattice sites, the activation energy for jumping from one site to the next may be large even if the geometrical constraints of the bottlenecks are small. Creation of strong bonding within the rigid network should make the bonding between alkali ion and network more ionic and hence, perhaps, less site-specific if the geometrical constraints at the bottlenecks are not a problem. There are two ways that the strength of the intranetwork bonding can be increased

* This work was sponsored by the Defense Advanced Research Projects Agency and NSF/RANN.

relative to the bonding between alkali ion and network: (1) The anions can bond with more than two cations of the network and (2) the anions can form strongly covalent bonds with a cation to make a complex anion. In a three-dimensional network, each anion must bond with at least two cations of the network. If the anions bond to four or more network cations, the network is close-packed and there is no passageway for interstitial alkali ions. If anions bond to three network cations, layer structures such as β-alumina may be anticipated. The low activation energy of β-alumina may be at least partly due to the fact that all the oxygen atoms neighboring the alkali ions, except those in sites 2c of space group $P6_3/mmc$, are bonded by three aluminum atoms that polarize the O^{2-}-ion charge density away from the alkali ion. If the oxygen atoms bond to only two network cations, polarization of the O^{2-}-ion charge density away from the alkali ions is reduced, thus increasing the activation energy for ion transport according to our hypothesis. Since two-dimensional transport was not of interest in this study, geometry restricts each anion to bonding with at most two network cations. Therefore, it seemed appropriate to build the network with at least one cation that formed a strongly covalent complex, thus utilizing in effect a complex anion such as SO_4^{2-}, NO_3^-, BO_3^{3-}, CO_3^{2-}, SiO_4^{4-}, or PO_4^{3-}. A tetrahedral complex seemed a logical starting place. The companion cation of the network can have a tetrahedral-site preference or an octahedral-site preference. The Carnegieite structure of high-temperature $NaAlSiO_4$, for example, has tetrahedrally coordinated Al^{3+} ions (1). In this work, the Zr^{4+} ion was chosen because it is stable in octahedral coordination and because zirconium oxides are not reduced by molten sodium.

This paper reports the synthesis and structural characterization of compounds in the system $Na_{1+x}Zr_2Si_xP_{3-x}O_{12}$, $0 \leq x \leq 3$, all of which can be reversibly ion-exchanged with Li^+, Ag^+, and K^+ ions in molten salts. The relationship of this work to a comprehensive investigation of skeleton structures is discussed in a companion paper (1), where preliminary transport measurements are also presented.

Experimental Procedure

The starting materials Na_2CO_3, ZrO_2 and $NH_4H_2PO_4$ were mixed in the Na-Zr-PO_4 ratios 212, 513, 123, 725, 547, and 759. The mixtures were preheated at 170° for 4 hours to decompose the $NH_4H_2PO_4$, at 900°C for 4 hours to decompose the Na_2CO_3, and overnight at 1200°C to transform any metaphosphate to orthophosphate. Normally, a metaphosphate decomposed to orthophosphate above about 1000°C (3). With the exception of mixes 513 and 725, the x-ray data of all products showed a single crystalline phase, as listed in Table 1. Interestingly, the mixes 212, 547, and 759 gave identical x-ray powder patterns having a somewhat smaller unit cell than that of mix 123. To obtain a single crystal of this dominant phase, a 212 mix was heated for 3 hours at 1600°C before the furnace was turned off. The crystals obtained for x-ray analysis by this procedure were typically cube-shaped, about 0.1 mm on a side. From the structure determination, the chemical composition was found to be $NaZr_2P_3O_{12}$. The structure consisted of an open network of $(PO_4)^{3-}$ tetrahedra coordinated octahedrally to Zr^{4+} ions with Na^+ ions filling a unique set of sites in a three-dimensionally linked interstitial space. The substitution of P^{5+} ions by $(Si^{4+} + Na^+)$ ions was attempted to introduce Na^+ ions into other positions of the interstitial space, an appropriate preparation of SiO_2 being added to the starting mix. Complete solid solution was found for the system $Na_{1+x}Zr_2Si_xP_{3-x}O_{12}$, $0 \leq x \leq 3$. Indeed, the end member $Na_4Zr_2Si_3O_{12}$ has previously been reported (4). X-ray data for compounds in this system are listed in Table 1. All structures were rhombohedral $R\bar{3}c$ except in the range $1.8 < x < 2.2$,

Table 1

X-ray Data for Compounds in the System $Na_{1+x}Zr_2Si_xP_{3-x}O_{12}$

Starting Composition	Space Group	a	b	c	β	V
$Na_2Zr(PO_4)_2$	$R\bar{3}c$	8.792(5)		22.723(9)		1521.0
$Na_5Zr_4(PO_4)_7$	$R\bar{3}c$	8.794(5)		22.721(9)		1522.7
$Na_7Zr_5(PO_4)_9$	$R\bar{3}c$	8.795(5)		22.722(9)		1523.2
$NaZr_2(PO_4)_3$	$R\bar{3}c$	8.815(1)		22.746(7)		1530.5
$Na_{1.4}Zr_2Si_{0.4}P_{2.6}O_{12}$	$R\bar{3}c$	8.840(3)		22.731(9)		1538.3
$Na_{1.8}Zr_2Si_{0.8}P_{2.2}O_{12}$	$R\bar{3}c$	8.898(1)		22.774(8)		1561.6
$Na_{2.2}Zr_2Si_{1.2}P_{1.8}O_{12}$	$R\bar{3}c$	8.940(3)		22.855(9)		1581.9
$Na_{2.6}Zr_2Si_{1.6}P_{1.4}O_{12}$	$R\bar{3}c$	8.980(5)		22.906(9)		1599.6
$Na_{2.8}Zr_2Si_{1.8}P_{1.2}O_{12}$	C 2/c	15.567(9)	9.003(5)	9.217(6)	123.76(5)	$1610.8 \times \frac{2}{3}$
$Na_{3.0}Zr_2Si_2PO_{12}$	C 2/c	15.586(9)	9.029(4)	9.205(5)	123.70(5)	$1616.6 \times \frac{2}{3}$
$Na_{3.2}Zr_2Si_{2.2}P_{0.8}O_{12}$	C 2/c	15.618(9)	9.051(6)	9.210(9)	123.93(6)	$1620.6 \times \frac{2}{3}$
$Na_{3.4}Zr_2Si_{2.4}P_{0.6}O_{12}$	$R\bar{3}c$	9.079(2)		22.685(9)		1619.3
$Na_{3.8}Zr_2Si_{2.8}P_{0.2}O_{12}$	$R\bar{3}c$	9.148(4)		22.239(9)		1611.6
$Na_4Zr_2Si_3O_{12}$*	$R\bar{3}c$	9.10		22.07		1583.9

* Ref. 4

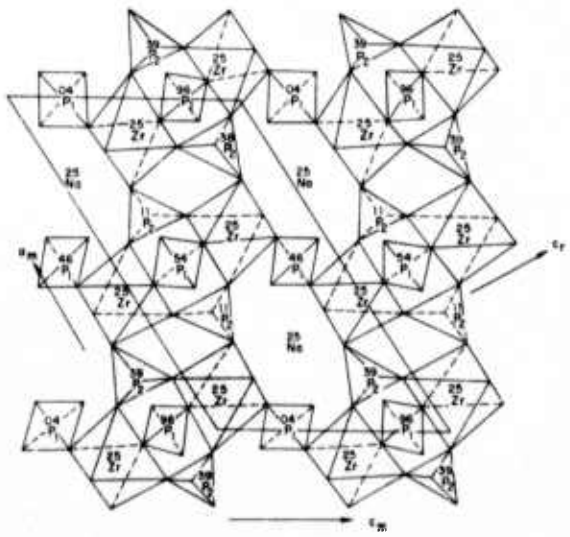

Fig. 1

Projection of half the unit cell along the a_r-axis of rhombohedral $NaZr_2P_3O_{12}$

Table 2

Final Atomic Parameters for $NaZr_2P_3O_{12}$ (Numbers in parentheses from Ref. 6)

Space group $R\bar{3}c$; cell parameter a = 8.815(1)Å, c = 22.746(7)Å

	x	y	z	β_{11}	β_{22}	β_{33}	β_{12}	β_{13}	β_{23}	β_0
Na	0	0	0	0.036(2)	0.022(1)	0.0010(2)	1/2 β_{11}	0	0	4.0(2) (4.2 ± 2)
Zr	0	0	0.14568(6) (0.1456 ± 1)	0.0036(2)	0.0036(2)	0.00023(3)	1/2 β_{11}	0	0	0.78(4) (1.80 ± 7)
P	0.2916(3) (0.2909 ± 6)	0	1/4	0.002(1)	0.0054(7)	0.00055(7)	1/2 β_{11}	0.0002(3)	1/2 β_{23}	1.08(7) (2.4 ± 1)
O(1)	0.1841(7) (0.1860 ± 15)	−0.0165(7) (−0.0144 ± 15)	0.1956(2) (0.1949 ± 5)	0.006(1)	0.008(1)	0.0006(1)	0.005(1)	0.006(3)	0.0001(3)	1.4(1) (3.2 ± 2)
O(2)	0.1911(8) (0.1913 ± 15)	0.1675(8) (0.1683 ± 15)	0.0876(2) (0.0866 ± 5)	0.007(1)	0.005(1)	0.0006(1)	0.003(1)	0.0004(3)	0.0000(3)	1.5(1) (2.9 ± 2)

where a distortion to monoclinic C2/c symmetry occurs. The structure of $NaZr_2P_3O_{12}$ was refined by single-crystal x-ray analysis. Attempts to grow single-crystal $Na_3Zr_2Si_2PO_{12}$ failed, but the distortion of the network is small enough that the network configuration in monoclinic $Na_3Zr_2Si_2PO_{12}$ could be deduced from powder data. Without single-crystal data, it is not possible to say anything definitive about the Na^+-ion distribution. However, there are Na_2 and Na_3 positions in addition to the Na_1 positions in the interstitial space that can accommodate the extra sodium.

An interesting feature of Table 1 is that the unit-cell size does not increase monotonically with x, as might be anticipated for a Si^{4+} radius of 0.40 Å vs a P^{5+} radius of only 0.31 Å. Rather, it reaches a maximum near x = 2.2, and the monoclinic C2/c phase is associated with the compositions having the largest rhombohedral c_r-axis, which produces the largest unit-cell volume.

Structure of $NaZr_2P_3O_{12}$

A cube-shaped crystal about 0.05 mm on an edge was selected for x-ray-diffraction analysis. Oscillation and Weissenberg photographs showed diffraction symmetry $\bar{3}$m. The systematic absences were $hk\ell$, $-h + k + \ell = 3n + 1$, and $h0\ell$ with $\ell = 2n + 1$, which is consistent with space groups R3c and R$\bar{3}$c. Three-dimensional intensity data to $2\theta = 50°$ were collected with Mo radiation as described elsewhere (5). In total, 705 reflections were measured. The heavy-atom method was used to solve the structure.

The true composition of the crystal was initially unknown. A strong peak at (0, 0, 0.29) in the Patterson map was assumed to represent an interaction between the Zr atoms. Therefore, twelve Zr atoms were assigned to the 12e positions at (0, 0, 0.145). From a Patterson map peak at (0, 0, 0.145), the Na atoms were assigned to the 6b positions at (0, 0, 0). A structure-factor calculation based on these positions gave a difference-function R value of 0.35. With this model and the assumption of R$\bar{3}$c symmetry, it was possible to identify from a difference Fourier synthesis one P atom and two O atoms. The atom parameters, scale factors, and anisotropic temperature factors were then refined with a full-matrix, least-squares program to give R = 0.043 and R_w = 0.060 for all reflections. The final values are listed in Table 2. Subsequently it was learned that Hagman and Kierkegaard (6) had reported the structure of $NaZr_2P_3O_{12}$. With the same space group, they obtained an R = 0.089. Their atomic parameters are listed in parentheses in Table 2. Both analyses gave high isotropic temperature factors for the Na^+ ions, indicating that these ions are mobile. In the present study, anisotropic temperature factors were refined. They show high mobility along the a_r axes, which are parallel to the tunnels of the interstitial space.

The structure consists of a three-dimensional skeletal network of PO_4 tetrahedra corner-sharing with ZrO_6 octahedra, the Na^+ ions occupying a large octahedral site in the interstitial space. Each ZrO_6 octahedra is connected to six PO_4 tetrahedra, while each tetrahedra is linked to four octahedra. A projection along the c_r-axis can be found in Ref. 6. The projection of half the unit cell along the a_r-axis, which permits visualization of the empty interstitial space inside the network, is shown in Fig. 1. The rhombohedral cell can also be indexed as a monoclinic cell with $a_m = 2a_r \sin 60° = 15.268$ Å, $b_m = a_r = 8.815$ Å, $c_m = c_r/3 \cos(\beta - 90) = 9.130$ Å, and $\beta = 123.85°$. The basic unit of the network, which is shaded in Fig. 1, consists of two octahedra joined by three tetrahedra, corresponding to $(Zr_2P_3O_{12})^-$. These units are connected so as to form a ribbon along the $[100]_m$ direction, and the ribbons are linked together by $P(1)O_4$

tetrahedra to form a two-dimensional sheet. The second half of the unit cell is a similar sheet with Zr atoms at $b_m = 0.75$ instead of $b_m = 0.25$ and displaced $c_m/2$, as indicated in Fig. 2. The Na atoms are located at Na_1 sites in $NaZr_2P_3O_{12}$. A $Na_1(25)$ is octahedrally coordinated by O^{2-} ions of the two neighboring $Zr(25)O_6$ octahedra. It is also octahedrally coordinated by 6 Na_2(rhomb) = 2 Na_2(mono) + 4 Na_3(mono) sites located in the same rhombohedral basal plane as the nearest-neighbor oxygen atoms. The bottleneck in the passageway from a Na_1 site to a Na_2 or Na_3 site is a puckered hexagonal ring having sides that alternate between octahedral and tetrahedral edges. The shortest diameter of the bottleneck is larger than 4.8 Å, twice the sum of Na^+-ion and O^{2-}-ion radii. Thus the geometrical features of the skeleton and its interstitial space satisfy the criteria for fast Na^+-ion transport, provided the site-preference energy for a Na_1 position is not too much greater than those for Na_2 or Na_3 positions.

Proposed Structure of $Na_3Zr_2Si_2PO_{12}$

As indicated in Table 1 the x-ray powder pattern of $Na_3Zr_2Si_2PO_{12}$ can only be indexed on a monoclinic cell. In the absence of single crystals, the single-crystal intensity data of $NaZr_2P_3O_{12}$ were reindexed on a monoclinic cell with $h_m = h_r - k_r$, $k_m = h_r + k_r$, and $\ell_m = (\ell_r - h_r + k_r)/3$. The positions of all atoms of single-crystal $NaZr_2P_3O_{12}$ were located from calculation of the Patterson map and, subsequently, of the difference Fourier map. The least squares refinement based on this new monoclinic space group C2/c gave the final atomic parameters listed in Table 3. An abnormally large isotropic temperature factor indicative of large thermal motion was observed along the b_m-axis, the only monoclinic axis parallel to a passageway between sodium sites (Na_1 and Na_3).

The proposed structure for $Na_3Zr_2Si_2PO_{12}$ is based on the following three assumptions: (1) the Si atoms are ordered in the P(2) positions, (2) the excess Na atoms are randomly distributed over positions 4e (0.50, 0.95, 0.25) and 8f (0.83, 0.10, 0.70), the Na_2 and Na_3 positions in Fig. 2, but electrostatic Na^+-Na^+ interactions and thermal motion make all the Na sites average positions with a large Debye-Waller factor, and (3) the network, though distorted and enlarged relative to $NaZr_2P_3O_{12}$, remains intact. The large, polyhedral sites Na_2 and Na_3 have Na-O distances greater than 2.4 Å, the sum of the Na^+ and O^{2-} ionic radii. Table 4 lists the bond distances calculated from powder data based on this proposed structure. The hexagonal bottlenecks between Na_1 and Na_2 or Na_3 positions are formed, as shown in Fig. 3, by three ZrO_6 octahedral edges alternating with three tetrahedral edges, one PO_4 and two SiO_4. The shortest diameter across this hexagon is 4.95 Å, which is larger than twice the sum of the Na^+ and O^{2-} ionic radii 4.8 Å. Each Na_2 or Na_3 site is connected through a bottleneck to two Na_1 sites, but there is no passageway between Na_2 sites or a Na_2 and a Na_3 site. The six channels through each Na_1 site provide a three-dimensionally linked interstitial space.

Ion Exchange of $NaZr_2P_3O_{12}$ and $Na_3Zr_2Si_2PO_{12}$

Characteristically, three-dimensional ionic conductors exchange alkali ions with a molten salt bath, the chemical concentration gradient acting as the driving force. Accordingly, powders of $NaZr_2P_3O_{12}$ and $Na_3Zr_2Si_2PO_{12}$ were held for four hours in molten $LiNO_3$, $AgNO_3$, and KNO_3, respectively. The powder:salt weight ratio was 1:20. The products were washed with water to remove the nitrates, dried, and analyzed by x-ray powder diffraction. The ion-exchanged cell parameters are listed in Table 5.

Table 3

Final Atomic Parameters for $NaZr_2P_3O_{12}$ and Proposed $Na_3Zr_2Si_2PO_{12}$

Space group C2/c; cell parameters for $NaZr_2P_3O_{12}$: a_m = 15.266(3)Å, b_m = 8.815(2)Å, c_m = 9.130(1)Å, β = 123.83(3)°

cell parameters for $Na_3Zr_2Si_2PO_{12}$: a_m = 15.58(9)Å, b_m = 9.029(4)Å, c_m = 9.205(5)Å, β = 123.7(5)°

	x	y	z	β_{11}	β_{22}	β_{33}	β_{12}	β_{13}	β_{23}	β_0
Na(1)	1/4	1/4	1/2	0.006(1)	0.017(2)	0.004(3)	0	0	0	3.8(2)
Zr	0.1043(1)	0.2498(2)	0.0629(2)	0.0009(1)	0.0019(2)	0.0015(2)	0.0000(1)	0.0002(1)	0.0000(1)	0.62(4)
P(1)	0	0.0412(8)	1/4	0.0017(5)	0.002(1)	0.004(1)	0	0.0016(7)	0	0.9(1)
P(2)	0.354(3)	0.1051(6)	0.2493(6)	0.0015(3)	0.0022(8)	0.004(1)	0.0000(3)	0.0011(5)	0.0000(8)	0.9(1)
O(1)	0.149(1)	0.43(1)	0.234(1)	0.003(1)	0.000(2)	0.004(2)	0.000(1)	0.001(1)	0.001(2)	1.2(2)
O(2)	0.438(1)	0.44(1)	0.088(1)	0.002(1)	0.004(2)	0.004(3)	0.000(1)	0.000(1)	0.001(2)	1.4(2)
O(3)	0.259(1)	0.172(1)	0.237(1)	0.0013(9)	0.003(2)	0.004(2)	0.000(1)	0.001(1)	0.003(2)	1.0(2)
O(4)	0.353(1)	0.144(1)	0.085(1)	0.003(1)	0.005(2)	0.004(3)	0.001(1)	0.002(1)	0.000(2)	1.4(2)
O(5)	0.453(1)	0.169(1)	0.412(1)	0.001(1)	0.005(2)	0.008(3)	0.002(1)	0.000(1)	0.000(2)	1.6(2)
O(6)	0.078(1)	0.139(1)	0.240(1)	0.0014(9)	0.001(2)	0.005(2)	0.000(1)	0.002(1)	0.002(2)	0.9(2)
Na(2)	0.50	0.95	1/4							
Na(3)	0.83	0.10	0.70							

Table 4

Bond Distances (Å) in Proposed Structure of $Na_3Zr_2Si_2PO_{12}$

Polyhedron around Na(1)		Polyhedron around Na(2)		Polyhedron around Na(3)	
Na(1)-O(1)	2 × 2.620	Na(2)-O(1)	2 × 2.413	Na(3)-O(1)	3.019
Na(1)-O(3)	2 × 2.599	Na(2)-O(4)	2 × 2.600	Na(3)-O(2)	3.031
Na(1)-O(6)	2 × 2.608	Na(2)-O(5)	2 × 2.808	Na(3)-O(2)	2.441
Na(1)-Na(2)	2 × 3.713	Na(2)-O(5)	2 × 2.974	Na(3)-O(3)	3.031
Na(1)-Na(3)	2 × 3.519	Na(2)-O(6)	2 × 3.081	Na(3)-O(3)	2.449
Na(1)-Na(3)	2 × 3.852	Na(2)-Na(1)	2 × 3.713	Na(3)-O(4)	2.621
Octahedron around Zr		Tetrahedron around P		Na(3)-O(4)	2.648
Zr-O(1)	2.104	PO-O(2)	2 × 1.542	Na(3)-O(5)	2.772
Zr-O(2)	2.077	PO-O(6)	2 × 1.546	Na(3)-O(6)	2.478
Zr-O(3)	2.142	Tetrahedron around Si		Na(3)-Na(1)	3.519
Zr-O(4)	2.055	Si-O(1)	1.583	Na(3)-Na(1)	3.852
Zr-O(5)	2.096	Si-O(3)	1.545	Na(3)-Na(3)	4.114
Zr-O(6)	2.137	Si-O(4)	1.543		
		Si-O(5)	1.546		

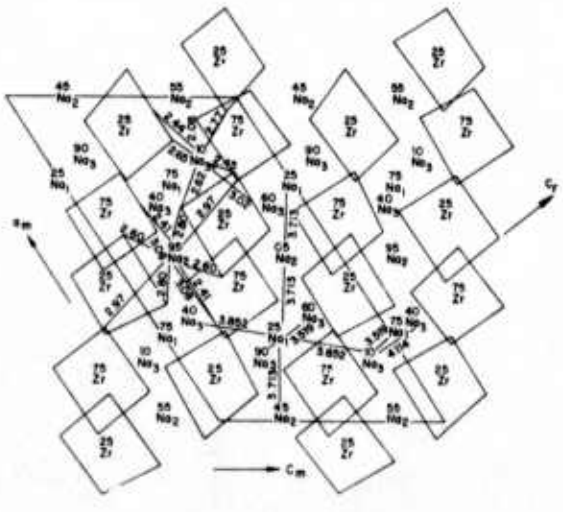

Fig. 2

Projection along the b_m-axis of the proposed monoclinic cell of $Na_3Zr_2Si_2PO_{12}$. Each Na(1) site is channeled three-dimensionally to two Na(2) sites and four Na(3) sites, and each Na(2) site or Na(3) site is linked to two Na(1) sites.

Replacement of the Na^+ ions by Li^+ ions in $NaZr_2P_3O_{12}$ tests the rigidity of the $(Zr_2P_3O_{12})^-$ network. Because the Li^+ ion is considerably smaller than the Na^+ ion, the network would be expected to collapse were it bonded tightly to the alkali ion. In fact, the network does not collapse. There is only a decrease in the unit-cell volume. Interestingly, the systematic increase in cell volume for $MZr_2P_3O_{12}$ on going from M = Li to Na to Ag to K in Table 5 is due to an increase in c_r, the parameter a_r actually decreasing slightly. From Fig. 1, the alkali ion occupies an M_1 position, which has as nearest neighbors two octahedral-site faces on opposite sides parallel to the basal plane. Clearly the spacing between these octahedral-site faces, and hence the size of c_r, will vary sensitively with the size of the M_1^+ cation. A tensile stretch along the c_r-axis is accompanied by a contraction in the basal plane. In $NaZr_2P_3O_{12}$, the Na_1-O distance is 2.6 Å, smaller than the sum of K^+ and O^{2-} ionic radii (2.75 Å), so an expansion of c_r must occur in $KZr_2P_3O_{12}$.

The situation is more complex for the series $M_3Zr_2Si_2PO_{12}$, where M = Li, Ag, and K. In the first place, only if M = Na is the space group monoclinic C2/c. In the second place, the c_r-axis for M = Li^+ is anomalously large, even though the cell volume is small, which indicates that the Li^+ ions occupy different positions in the interstitial space. The most probable position would be at a bottleneck, since this would allow the shortest Li-O distances. Such a conjecture is supported by the anomalous variation with x of the lattice parameters for the system $Na_{1+x}Zr_2Si_xP_{3-x}O_{12}$ given in Table 1. The fact that "c_r" is a maximum near x = 2.2 is compatible with electrostatic repulsions between Na^+ ions forcing displacement toward the bottleneck positions, thus contributing to the large Debye-Waller factor. Hybridization of the $4d^{10}$ core orbitals with empty 5s and 5p orbitals at a Ag^+ ion would permit it to accommodate to a bottleneck position (7), and it appears from Table 5 that the Ag^+-ion distribution is similar to the Na^+-ion distribution. The larger K^+ ions, on the other hand, would not be so easily accommodated in the bottleneck positions, and smaller K^+-ion displacements are compatible with Table 5.

Because the energy of hybridization at a Ag^+ ion is comparable to the increased covalent-bond energy made possible in oxides by hybridization, the Ag-O bond length may vary over quite a range from compound to compound. Shorter bond lengths signal hybridization and a stronger covalent component, which results in turn in a darkening of the crystal (7). If a silver oxide is white, the Ag-O distance is longer than 2.4 Å and the bond is largely ionic. As the Ag-O distance shortens, the color of the silver oxide changes from white to yellow to orange to brown to black. Therefore, if ion-exchange with Ag^+ ions produces a dark product, two inferences can be made: (1) the intranetwork bonding is not strong enough to inhibit hybridization at the Ag^+ ion with formation of a strong covalent contribution to the Ag-O bond and (2) it may not be possible to reverse ion-exchange from Ag^+ to Na^+ because of the tight Ag-O bond. In such a case, the Na-O bonding is expected to be strong enough to make the activation energy for Na^+-ion transport relatively larger. The $AgZr_2P_3O_{12}$ obtained from ion-exchanged $NaZr_2P_3O_{12}$ in molten $AgNO_3$ is white, indicating ionic Ag-O bonding and strong intranetwork bonding. This observation is consistent with the lattice-parameter variations of Table 5. The color of $Ag_3Zr_2Si_2PO_{12}$, on the other hand, is light yellow, indicating that at least some of the Ag^+ ions have an appreciable covalent contribution to some Ag-O bonds. Such would be the case were some Ag^+ ions displayed toward the bottleneck positions. The fact that the Ag compound can be reverse ion-exchanged indicates that the covalent contribution to the Ag-O bond is not too strong.

Table 5

X-ray Data for Ion-exchanged $NaZr_2P_3O_{12}$ and $Na_3Zr_2Si_2PO_{12}$

Compound	Space Group	a(Å)	b(Å)	c(Å)	β(°)	V(Å)^3
$LiZr_2P_3O_{12}$	$R\bar{3}c$	8.817(5)		22.561(9)		1518.8
$NaZr_2P_3O_{12}$	$R\bar{3}c$	8.815(1)		22.746(7)		1530.5
$AgZr_2P_3O_{12}$	$R\bar{3}c$	8.814(1)		22.889(7)		1539.8
$KZr_2P_3O_{12}$	$R\bar{3}c$	8.810(1)		23.841(9)		1566.5
$Li_3Zr_2Si_2PO_{12}$	$R\bar{3}c$	8.554(5)		23.314(9)		1477.4
$Na_3Zr_2Si_2PO_{12}$	C 2/c	15.586(9) (9.029)	9.029(4)	9.205(5) (22.974)	123.70(5)	1616 × 2/3
$Ag_3Zr_2Si_2PO_{12}$	$R\bar{3}c$	9.058(3)		23.059(9)		1638.5
$K_3Zr_2Si_2PO_{12}$	$R\bar{3}c$	8.940(3)		23.721(9)		1641.8

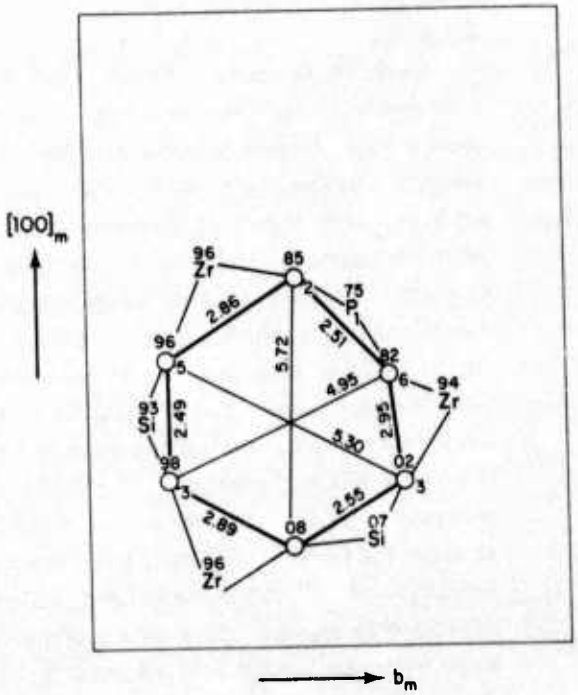

Fig. 3

A "bottleneck" of $Na_3Zr_2Si_2PO_{12}$ formed by three ZrO_6-octahedral edges and three (two SiO_4 and one PO_4) tetrahedral edges with a shortest diameter of 4.95 Å.

The fact that the compounds can be reverse ion-exchanged with K^+ ions shows that the bottlenecks are large enough to permit the large K^+ ions to pass. Therefore, we anticipate fast Na^+-ion conduction in the system $Na_{1+x}Zr_2Si_xP_{3-x}O_{12}$.

Discussion

The system $Na_{1+x}Zr_2Si_xP_{3-x}O_{12}$ has a skeleton structure consisting of a rigid, three-dimensional network stabilized by electrons from mobile alkali ions in a three-dimensionally linked interstitial space. As such, it is one of a class of compounds showing promise for fast ion conduction (1). In general, such structures are plagued by the fact that the interstitial space may accept, in addition to the alkali ions of interest, small molecules like H_2O or Na_2O that block alkali-ion transport (1). Indeed, this problem is also common to β-alumina (8). The system under study here does not become hydrated, but there is some evidence that excess Na_2O may be incorporated. The cell parameters obtained from the original 212, 547, and 759 mixes, which contained an excess of Na_2O, were different (see Table 1) from those of the single crystal, which was grown from a 212 mix fired for a few hours at a high enough temperature (1600°C) to drive off excess Na_2O. The single-crystal data gave no evidence of excess Na_2O.

In $NaZr_2P_3O_{12}$, the Na_1 positions are filled and the Na_2 positions are empty. Since the site-preference energies for the two positions are not equal, the activation energy for Na^+-ion conduction may be large. In the system $Na_{1+x}Zr_2Si_xP_{3-x}O_{12}$, on the other hand, the introduction of excess Na^+ ions introduces electrostatic Na^+-Na^+ interactions that can lower the activation energy even though transport must be via a Na_1 site. The structural evidence for displacement of Na^+ ions toward bottleneck positions in $Na_3Zr_2Si_2PO_{12}$ indicates that this is the case, and indeed the transport properties at 300°C are comparable to those of the best β''-alumina (1).

In closing, it is interesting to compare the properties of $Na_3Zr_2Si_2PO_{12}$ investigated here with those of β-alumina.

(1) In both compounds, the Na^+ ions can be exchanged reversibly in molten salts with Li^+, Ag^+, and K^+ ions.

(2) In both compounds, the lattice parameters of the Li^+-exchanged products indicate that the Li^+ ions occupy different lattice positions than the Na^+ ions.

(3) In both compounds, available alkali-ion positions are crystallographically inequivalent, and the total number of positions is only partially occupied.

(4) In $Na_3Zr_2Si_2PO_{12}$ the bottleneck to M^+-ion transport is a hexagon with a shortest Na-O contact of 2.475 Å; in β-alumina it is a rectangle between sites 2b and 2d of $P6_3/mmc$ with a shortest Na-O contact of 2.71 Å, and the 2b position itself is a midpoint between two O^{2-} ions separated by 4.84 Å.

(5) In β-alumina, the Na^+ ions are constrained to two-dimensional motion; in $Na_3Zr_2Si_2PO_{12}$ they move in three dimensions and the Na-site density is twice as large: 11.13 vs 5.57 × 10^{21} cm^{-3}.

(6) Whereas β-alumina has an anisotropic thermal expansion, pseudocubic $Na_3Zr_2Si_2PO_{12}$ may have a nearly isotropic thermal expansion, thus minimizing thermally induced stresses at grain boundaries of a ceramic membrane.

(7) Both compounds are stable in molten sodium.

(8) Ceramic processing of $Na_3Zr_2Si_2PO_{12}$ can be achieved at around 1200°C, substantially below the 1500°C needed for β-alumina.

I would like to thank J. B. Goodenough for fruitful discussions throughout the course of this work and for a critical reading of the manuscript, C. H. Anderson for technical assistance with the experiments.

REFERENCES

1. J. B. Goodenough, H. Y-P. Hong, and J. A. Kafalas, Companion Paper.
2. H. Y-P. Hong, Acta. Cryst. B30, 945 (1974).
3. H. Y-P. Hong, Mat. Res. Bull. 10, 635 (1975).
4. R. G. Sizova, A. A. Voronkov, N. G. Shumyatskaya, V. V. Pyakhim, and N. V. Belov, Dokl. Akad. Nauk SSSR, Ser. 205, Issue 1, 90 (1972).
5. H. Y-P. Hong, Acta. Cryst. B30, 468 (1974).
6. L. Hagman and P. Kierkegaard, Acta. Chem. Scan. 22, 1822 (1968).
7. H. Y-P. Hong, J. A. Kafalas, and J. B. Goodenough, J. Sol. State Chem. 9, 345 (1974).
8. W. L. Roth, W. C. Hamilton, and S. J. Laplace, Am. Cryst. Assoc. Abstr., Ser. 2, 1, 169 (1973).

DISTRIBUTION LIST

T. R. Beck
Flow Research, Inc.
1819 S. Central Ave., Suite 72
Kent, Washington 98031

S. J. Begun
Gould, Inc.
4000 International Tower Bldg.
Chicago, Illinois 60631

James Birk
Electric Power Research Institute
Palo Alto, California 94304

J. Boechler
Technical Librarian
Electrochimica Corporation
2485 Charleston Road
Mountain View, California 94040

J. Broadhead
Bell Telephone Laboratories
600 Mountain Avenue
Murray Hill, New Jersey 07974

Charles T. Brown
Chemical Sciences Section
United Aircraft Research Laboratories
East Hartford, Connecticut 06108

Stanley Bruckenstein
Department of Chemistry
State University of New York
Buffalo, New York 14214

Paul F. Chenea
General Motors
12 Mile and Mound Roads
Warren, Michigan 48090

Capt. Wayne Clements
AFDL
Wright-Patterson AFB, Ohio 45433

Cortland O. Dugger
Hq. AFSC/DLCEC
Andrews AFB, Maryland 20334

Denton W. Elliott
Department of the Air Force
Air Force Office of Scientific
Research (AFSC)
1400 Wilson Boulevard
Arlington, Virginia 22209

I. Wynn Jones
Electricity Council Research Centre
Capenhurst, Chester, England

M. Klein
Energy Research Corporation
Bethel, Connecticut 06801

John J. Lander
AFSC/POE
Wright-Patterson AFB, Ohio 45433

C. Liang
P. R. Mallory and Co. Inc.
Laboratory for Physical Sciences
Burlington, Massachusetts 01803

David M. Mason
Stanford University
Department of Chemical Engineering
Stanford, California

P. Morgatin
Compagnie Generale d'Electricite
Marcoussis, France

Donald Mortel
AFSC/POE
Wright-Patterson AFB, Ohio 45433

John Mysing
AFAL/AAA
Wright-Patterson AFB, Ohio 45433

Robert A. Osteryoung
Department of Chemistry
Colorado State University
Ft. Collins, Colorado 80521

J. V. Petrocelli, Manager
Chemical Engineering Department
Scientific Research Staff
Ford Motor Company, P. O. Box 2053
Dearborn, Michigan 48121

Thomas B. Reddy
Sponsored Research Section
American Cyanamid Company
Stamford Research Laboratories
1937 West Main Street
Stamford, Connecticut 06904

Walter Roth
General Electric Company
Corporate Research and
Development Laboratories
Schenectady, New York 12301

W. M. Rouquemore
AFAPL/SFF-2
Wright-Patterson AFB, Ohio 45433

Stanley Ruby
Materials Sciences
Defense Advanced Research
Projects Agency
1400 Wilson Boulevard
Arlington, Virginia 22209

Richard I. Schoen
Program Manager
Advanced Energy Research and
Technology Division
National Science Foundation
Washington, D. C. 20550

Herbert P. Silverman
TRW Systems, Inc.
1 Space Park
Redondo Park, California 90278

Joseph Singer
Chemistry Section
Energy Conversion and Environmental
Systems Division
NASA Lewis Research Center
Cleveland, Ohio 44135

C. Martin Stickley
Director for Materials Science
Advanced Research Projects Agency
1400 Wilson Boulevard
Arlington, Virginia 22209

John A. Swartout
Union Carbide
270 Park Avenue
New York, N. Y. 10017

Floris Y. Tsang
The Dow Chemical Company
Walnut Creek, California 94596

K. Wang
Electrochimica Corporation
Mountain View, California 94040

Don R. Warnock
AFSC/POE
Wright-Patterson AFB, Ohio 45433

Nicholas Winograd
Department of Chemistry
Purdue Research Foundation
Lafayette, Indiana 47907

M. Stanley Whittingham
Corporation Research Laboratories
EXXON Research and Engineering
P. O. Box 45
Linden, New Jersey 07036

UNCLASSIFIED

SECURITY CLASSIFICATION OF THIS PAGE *(When Data Entered)*

REPORT DOCUMENTATION PAGE

READ INSTRUCTIONS BEFORE COMPLETING FORM

1. REPORT NUMBER: NSF/[redacted] 74-02094 SR-2/75; ESD-TR-76-29
2. GOVT ACCESSION NO.
3. RECIPIENT'S CATALOG NUMBER
4. TITLE *(and Subtitle)*: Solid Electrolytes: Alkali-Ion Transport in Skeleton Structures
5. TYPE OF REPORT & PERIOD COVERED: Second Semiannual Technical Summary [redacted] no. 2
6. PERFORMING ORG. REPORT NUMBER: 1 Jul - 31 Dec 75
7. AUTHOR(s): J. B. Goodenough, H. Y-P. Hong, J. A. Kafalas, [redacted] K. Dwight
8. CONTRACT OR GRANT NUMBER(s): NSF/RANN AER 74-02094; F19628-76-C-0002; ARPA Order-2696
9. PERFORMING ORGANIZATION NAME AND ADDRESS: Lincoln Laboratory, M.I.T., P.O. Box 73, Lexington, MA 02173
10. PROGRAM ELEMENT, PROJECT, TASK AREA & WORK UNIT NUMBERS: Program Element No. 61101E; Project Code No. 6D10
11. CONTROLLING OFFICE NAME AND ADDRESS: Defense Advanced Research Projects Agency, 1400 Wilson Boulevard, Arlington, VA 22209; National Science Foundation, RANN Directorate, Washington, DC 20550
12. REPORT DATE: 31 Dec [redacted] 75
13. NUMBER OF PAGES: 44
14. MONITORING AGENCY NAME & ADDRESS *(if different from Controlling Office)*: Air Force Office of Scientific Research, 1400 Wilson Boulevard, Arlington, VA 22209
15. SECURITY CLASS. *(of this report)*: Unclassified
15a. DECLASSIFICATION DOWNGRADING SCHEDULE
16. DISTRIBUTION STATEMENT *(of this Report)*: Approved for public release; distribution unlimited.
17. DISTRIBUTION STATEMENT *(of the abstract entered in Block 20, if different from Report)*
18. SUPPLEMENTARY NOTES: None
19. KEY WORDS *(Continue on reverse side if necessary and identify by block number)*: solid electrolytes; sodium-sulfur batteries; alkali-ion transport; fast ion transport
20. ABSTRACT *(Continue on reverse side if necessary and identify by block number)*

We have demonstrated the existence of fast, three-dimensional Na^+-ion transport in the system $Na_{1+3y}Zr_2(P_{1-y}Si_yO_4)_3$ for $0 \leq y \leq 1$. At 300°C, the operating temperature of a Na-S battery, the resistivity (5 Ω-cm) for Na^+-ion transport in $Na_3Zr_2PSi_2O_{12}$ is competitive with the best β"-alumina. The activation energy for Na^+-ion transport, about 0.26 eV, is about 0.08 eV higher than that of β"-alumina, which makes this compound superior to the best β"-alumina at temperatures greater than 300°C, inferior at lower temperatures. The compound is stable in molten sodium and can be sintered at 1250°C. We have elected to concentrate on the fabrication of ceramic cups suitable for cell construction in order to test the chemical stability of this compound under the operating conditions of a Na-S cell.

DD FORM 1 JAN 73 1473 EDITION OF 1 NOV 65 IS OBSOLETE

UNCLASSIFIED

SECURITY CLASSIFICATION OF THIS PAGE *(When Data Entered)*

DEGREE

LESS THAN OR EQUAL TO

DEGREE

207650